

# X-ray (absorption) spectroscopy and data-analysis



SOCIETÀ ITALIANA LUCE DI SINGROTRONE  
ITALIAN SYNCHROTRON RADIATION SOCIETY  
www.synchrotron-radiation.it

Andrea Di Cicco

*Physics Division, School of Science and Technology,  
Università di Camerino*



# Current strategies for data-analysis

In (very) brief:

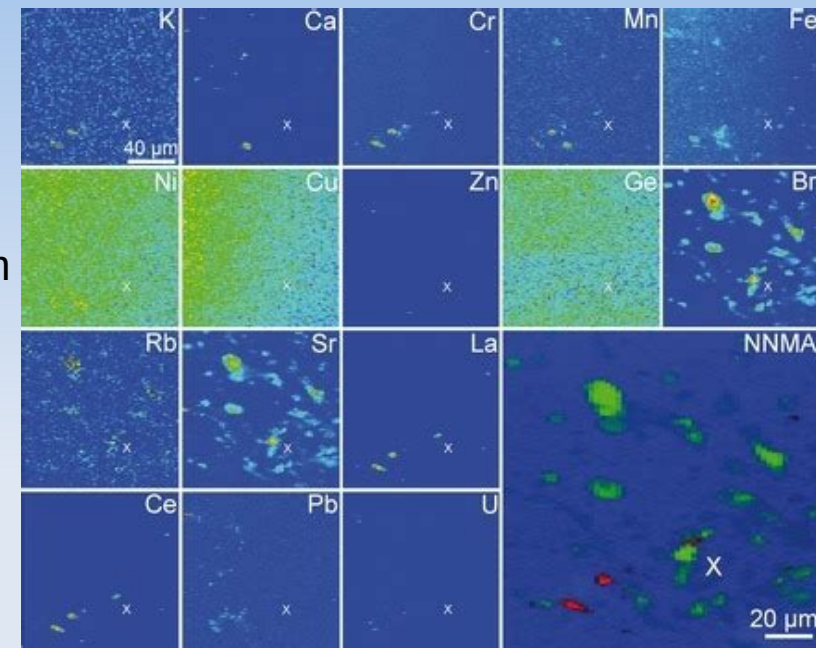
- 1) X-ray fluorescence spectroscopy: peak-fitting techniques for qualitative and quantitative analysis.
- 2) *X-ray absorption spectroscopy: mainly refinements using advanced simulation techniques (typically multiple-scattering calculations)*. For XANES calculations follow the Benfatto's lecture.
- 3) For x-ray absorption near-edge structures of real materials other empirical approaches are often used such as pre-edge peak fitting, linear combination of standards and principal component analysis (follow also the next Meneghini's lecture).

# Peak-fitting of XRF spectra

→ XRF spectra of dense samples can be collected in few milliseconds with modern X-ray sources and solid-state detectors. 2- or even 3-dimensional maps of XRF data can be collected, with each pixel in the map holding an XRF spectrum.

→ **Peaks correspond to characteristic X-ray emission lines** from the elements. Furthermore, the intensity of each peak can be used to infer the concentration.

→ XRF spectra are relatively easy to interpret: the characteristic emission energies for each atom are well known to high precision and the absorption and emission probabilities are known to pretty good precision. In this sense, a crude approach to XRF analysis is to use the area under the appropriate peaks as a quantifiable value for the elements abundance.



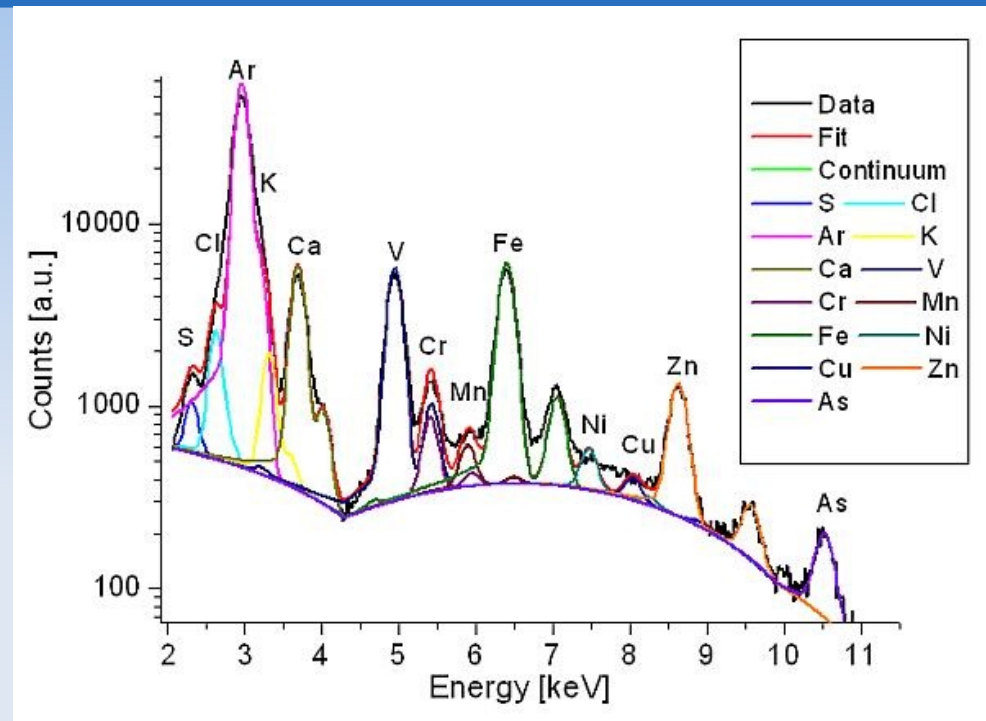
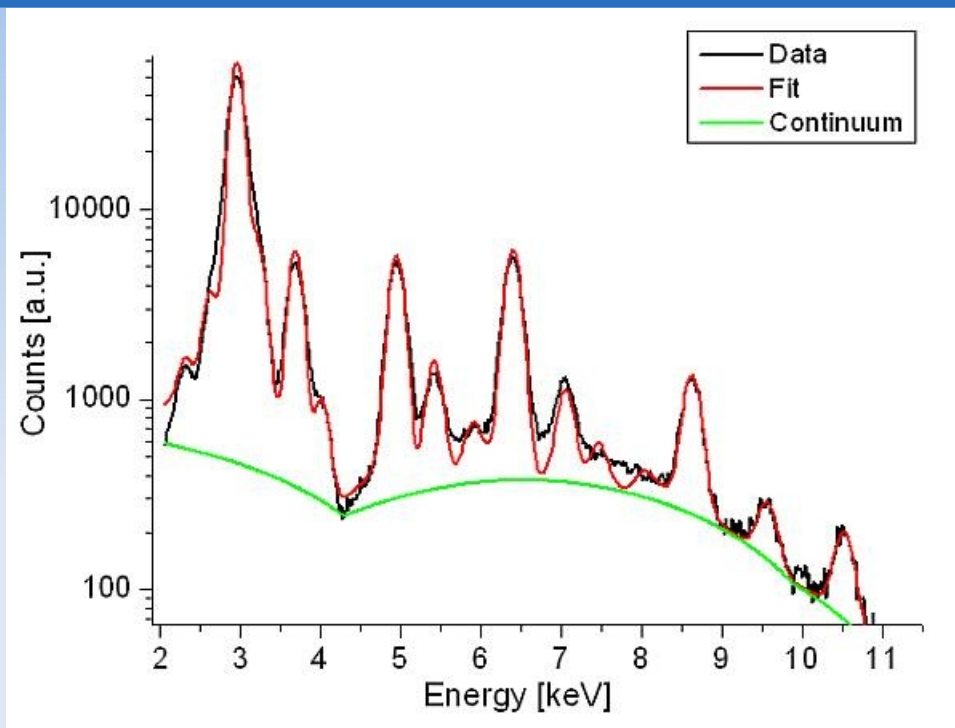
SR-XRF map of fluid inclusions in U deposits

→ The *complications for quantitative analysis* of XRF spectra are due mostly to:

1. Photon-in photon-out x-ray attenuation effects in the sample (high and non-linear dependence on the atomic number of the elements  $\mu \sim Z^4 E^{-3}$ ).
2. Overlaps of elemental peaks which is also favored by the relatively poor resolution of solid detectors.
3. Detector response and artefacts. Resolution, quantum efficiency and saturation effects can affect and distort collected spectra.

Quantitative analysis can be performed by most commercial softwares associated with solid-state detector multichannel chains. To be used with caution but reasonable results in most cases.

# Peak-fitting elemental analysis



The usual refinement strategy for XRF spectra is to reproduce the experimental spectra by adapting a background shape (usually a piecewise polynomial function) and a series of distinct peaks typically represented by Gaussian functions. The parameters of the Gaussian functions are simply related to the peak positions, which correspond to well-defined elemental x-ray emission energies. In figure we have a composite sample. The width of the peaks is usually associated with the detector resolution, while the intensities (area) of the peaks are related to the amount of selected atomic species. Specialized commercial software are usually available for such analysis.

Elastic and inelastic Compton scattering components near the excitation energy are also detected. Strong components may be partially attenuated by filters.

# The XAS fine structure

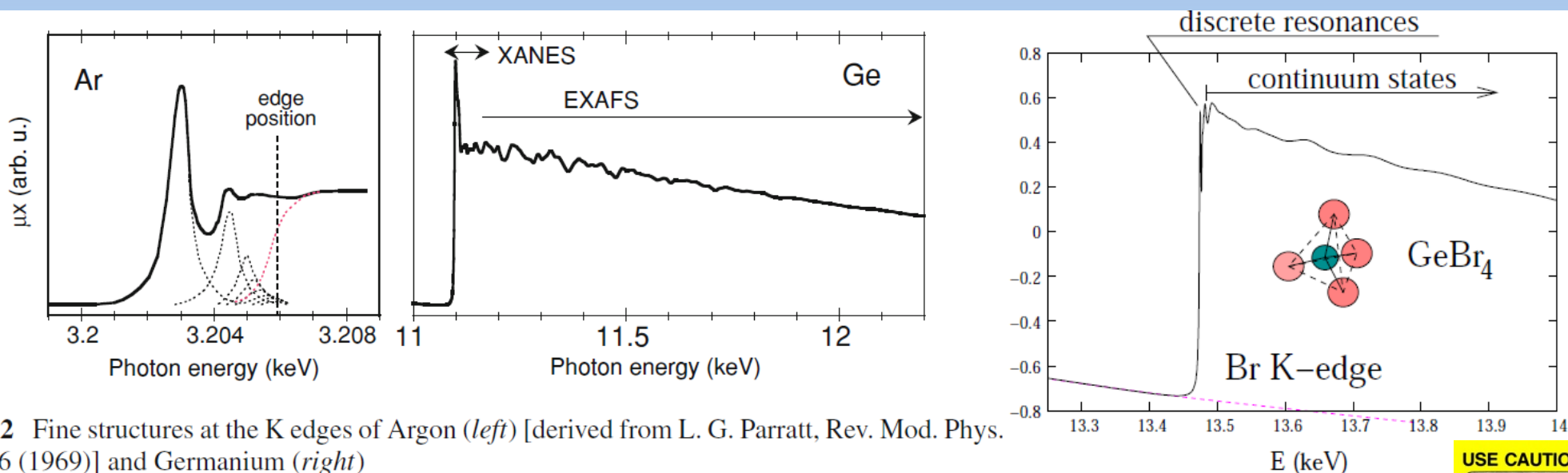
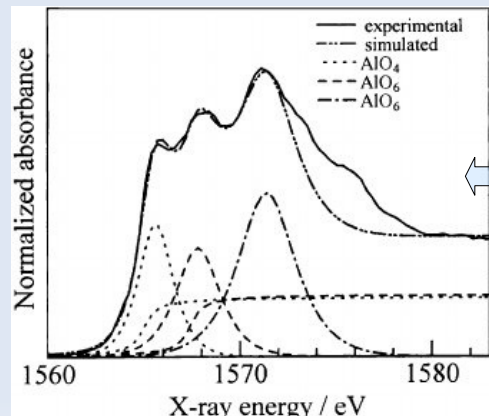


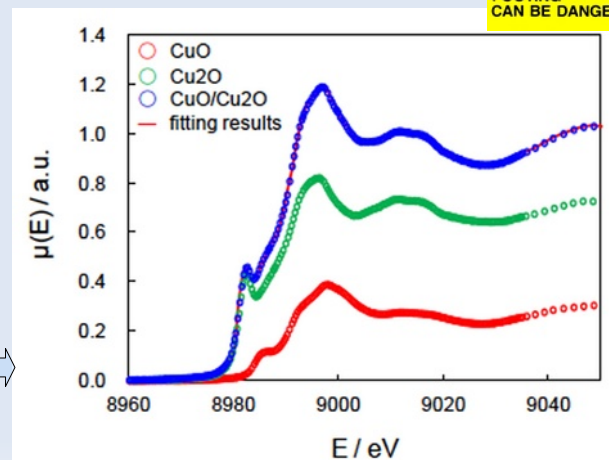
**Fig. 6.2** Fine structures at the K edges of Argon (*left*) [derived from L. G. Parratt, Rev. Mod. Phys. 31, 616 (1969)] and Germanium (*right*)

Near-edge (XANES): full multiple-scattering simulations (muffin-tin or beyond muffin-tin approximations). In complex real materials empirical approaches are often used such as pre-edge peak fitting, linear combination of standards and principal component analysis.



Distinct multiplet energies are quite robustly correlated with electronic and local atomic structure of the metal and its ligands. Peak-fitting with Lorentzian, Gaussian or Voigt functions. The energy resolution of XANES measurement continues to improve, so this is becoming a clearer and a richer resource for spectral analysis.

Spectra of complex substances may be reproduced by linear combinations of standards like in this simple case of a mixture of CuO and CuO<sub>2</sub> oxides.





# Modern XAS data-analysis

The absorption coefficient ( $\alpha$  in figure) is modelled as a sum of different contributions including background and properly normalized structural signals:

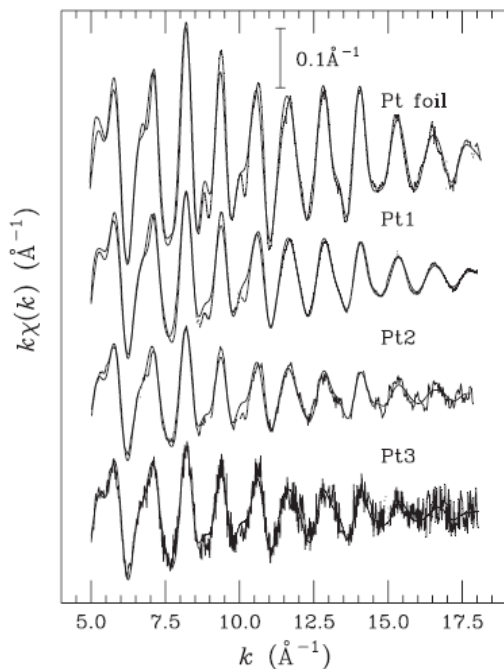
$$(32) \quad \alpha_m(E_i) = \alpha_{bkg}(E_i) + \alpha_{exc}(E_i) + [1 + \chi_m(E_i)] \alpha_0(E_i)$$

where

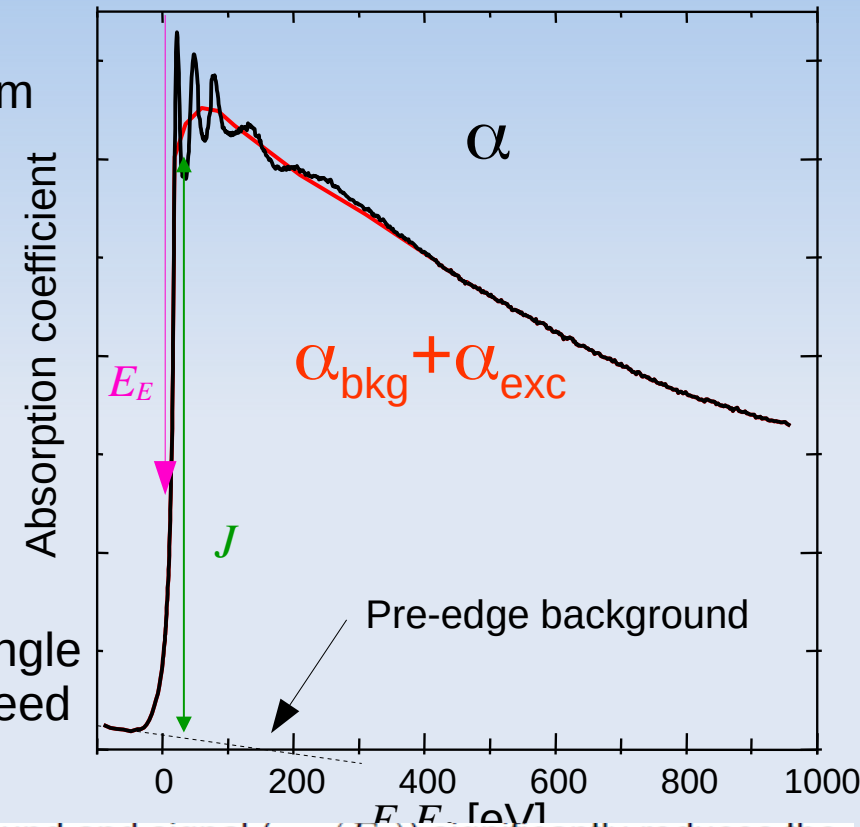
$\alpha_0(E_i) = J\sigma_0(E_i)$  is the atomic absorption coefficient

$\alpha_{bkg}(E_i)$  is a smooth polynomial background

$\alpha_{exc}(E_i)$  accounts for multi-electron excitation channels



Structural and non-structural parameters are refined in a single minimization procedure. No need of Fourier filtering.



Simultaneous modelling of background and signal ( $\chi_m(E_i)$ ) significantly reduces the introduction of systematic errors in the interpretation of the structural signal.

Same approach for multi-edge studies:

$$(33) \quad \alpha_m(E_i) = \alpha_{bkg}(E_i) + \alpha_{exc}(E_i) + \sum_{j=1}^{NXAS} [1 + \chi_m^j(E_i)] \alpha_0^j(E_i)$$

# Background: multi-electron excitations

- Multi-electron excitation channels: contribution may be of the order of 1% of the single-electron (main) channel. Realistic calculations of those channels are extremely difficult, only energy onsets can be reproduced accurately.
- Various model functions have been tested and used (within GNXAS). Inclusion is necessary to get quantitative agreement with the data.
- Multielectron excitations were studied in a variety of cases (3<sup>rd</sup> to 6<sup>th</sup> period Elements) also using photoemission spectroscopy.
- Very important for disordered systems (weaker XAS signal).

## AgBr (solid and liquid)

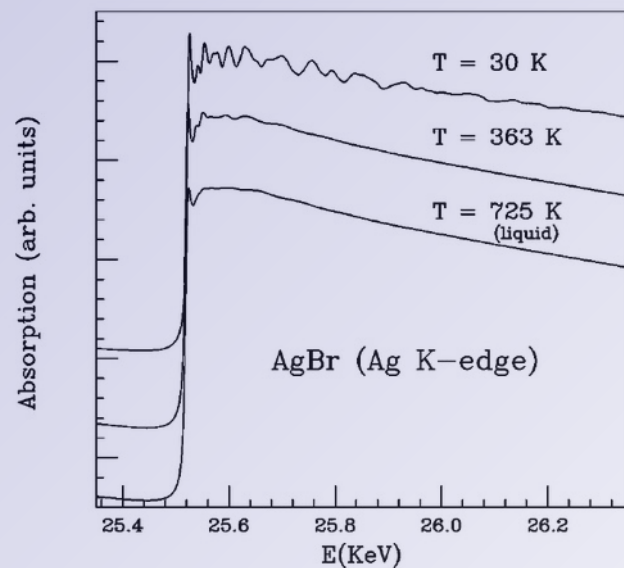
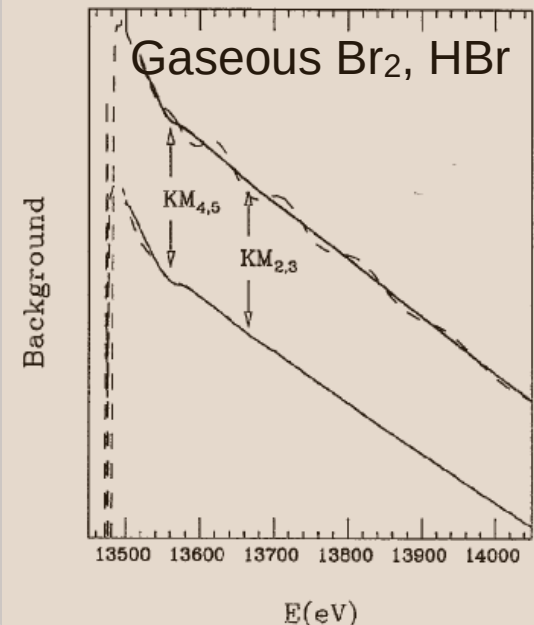
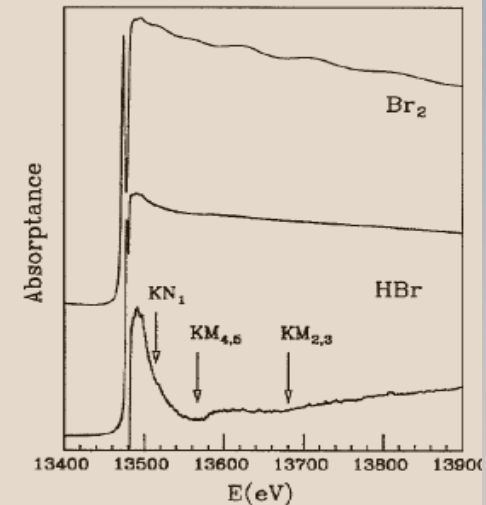
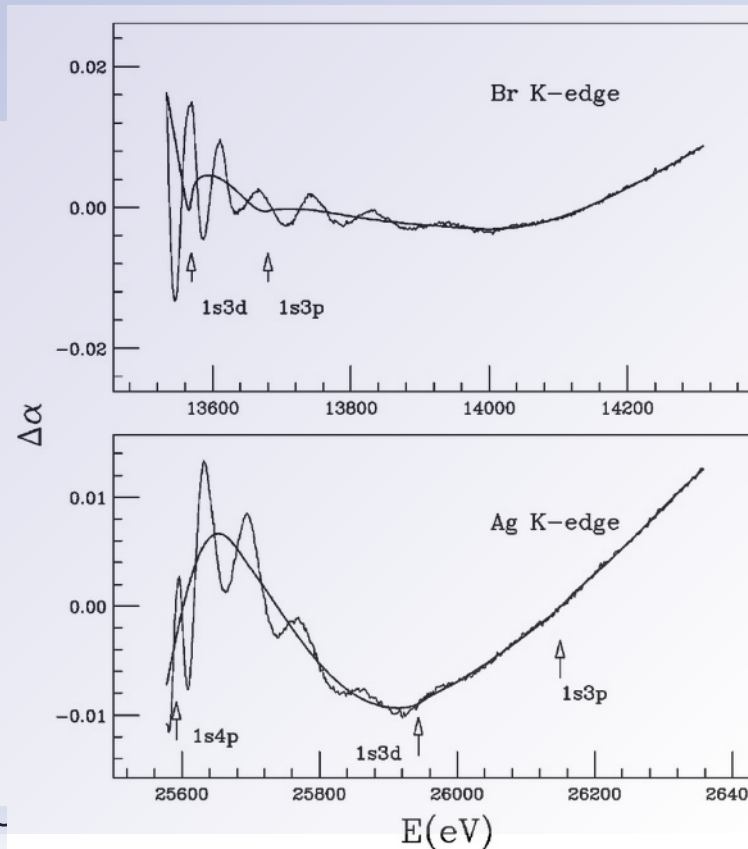


FIG. 3. X-ray absorption spectra of AgBr near the Ag K-edge are shown for three different temperatures in the solid and liquid phases.



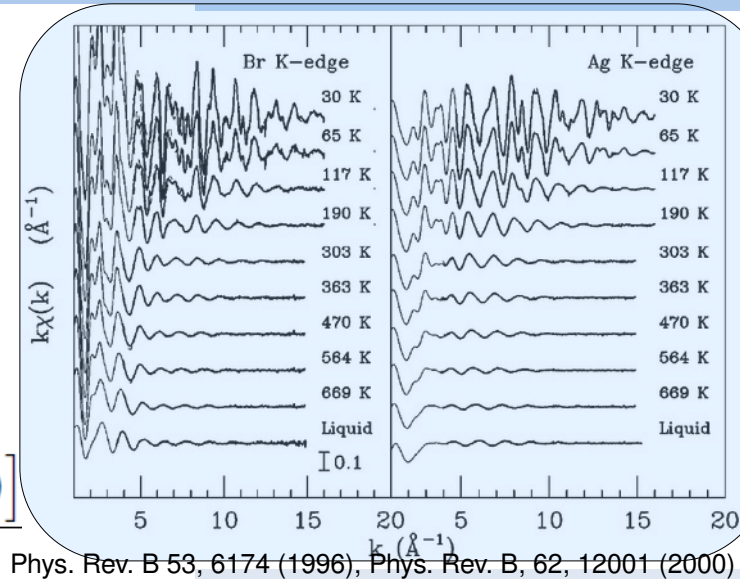
# XAS structure refinement

The experimental structural signal is thus defined as:

$$(34) \quad \chi(E_i) = \frac{[\alpha(E_i) - \alpha_{bkg}(E_i) - \alpha_{exc}(E_i)]}{\alpha_0(E_i)}$$

or for multi-edge

$$(35) \quad \chi(E_i, j) = \frac{[\alpha(E_i) - \alpha_{bkg}(E_i) - \alpha_{exc}(E_i) - \sum_{l \neq j} J_l \sigma_{nor}(E_i, l) \chi(E_i, l)]}{\sigma_{nor}(E_i, j) \times J_j}$$



Phys. Rev. B 53, 6174 (1996), Phys. Rev. B, 62, 12001 (2000)

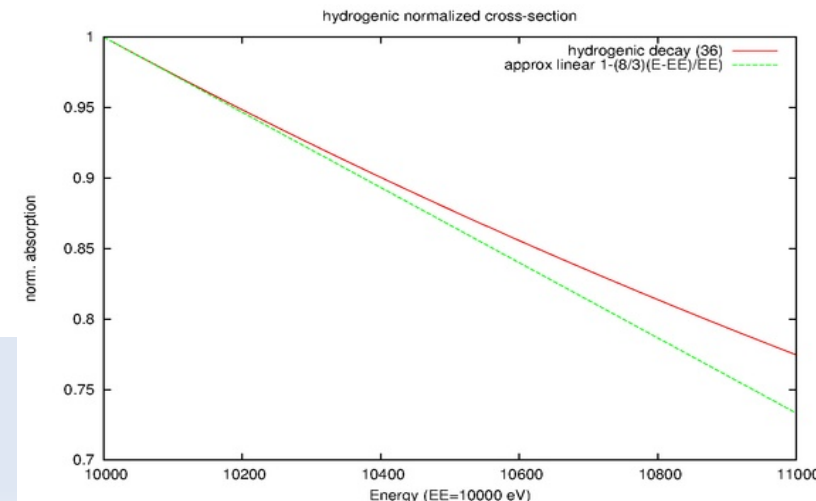
AgBr for  
Increasing temperature

Normalization to the atomic cross-section is performed using a standard hydrogen-like absorption function  $\sigma_{nor}(E_i)$ ,  $\sigma_{nor}(E_i) \times J = \alpha_0(E_i)$ :

$$(36) \quad \sigma_{nor}(E_i) = \frac{1}{e^{-4}} e^{(-4 \times \arctan \frac{1}{\eta})} \times \frac{1}{\left(1 + \frac{1}{\eta^2}\right)^4} \times \frac{1}{1 - e^{-2\pi\eta}}$$

where  $\eta^2 = \frac{EE}{(E_i - EE)}$ . Lengeler and P. Eisenberger, Phys. Rev. B 21, 4507 (1980)

Phys. Rev. B 52, 15135 (1995) -see refs. therein





# Refinement procedures

- The function  $R$  which is minimized in the program is the sum over  $i = 1, N$  points of the squares of the differences between model and experimental signals in the specified energy interval times a weight function:

$$(37) \quad R = \sum_i [\alpha(E_i) - \alpha_m(E_i, \{\lambda\})]^2 \times W(E_i)$$

Here the model signal  $\alpha_m(i)$  depends on the ensemble of structural parameters  $\{\lambda\}$ . The weighting function  $W(E_i)$  is calculated as:

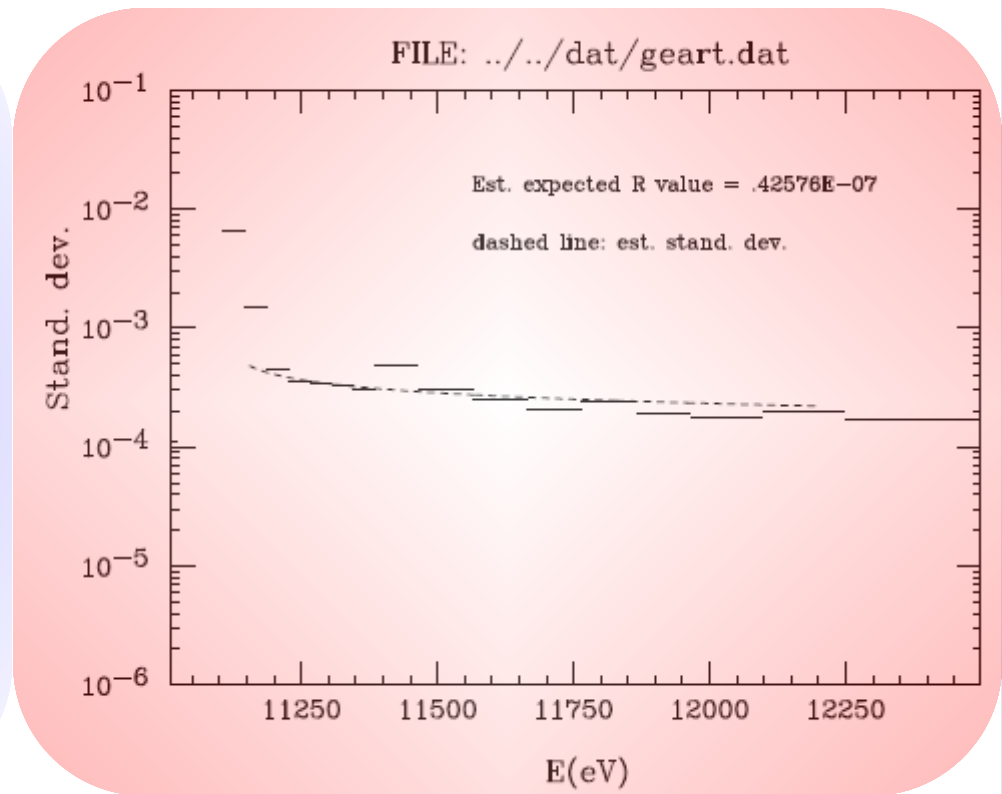
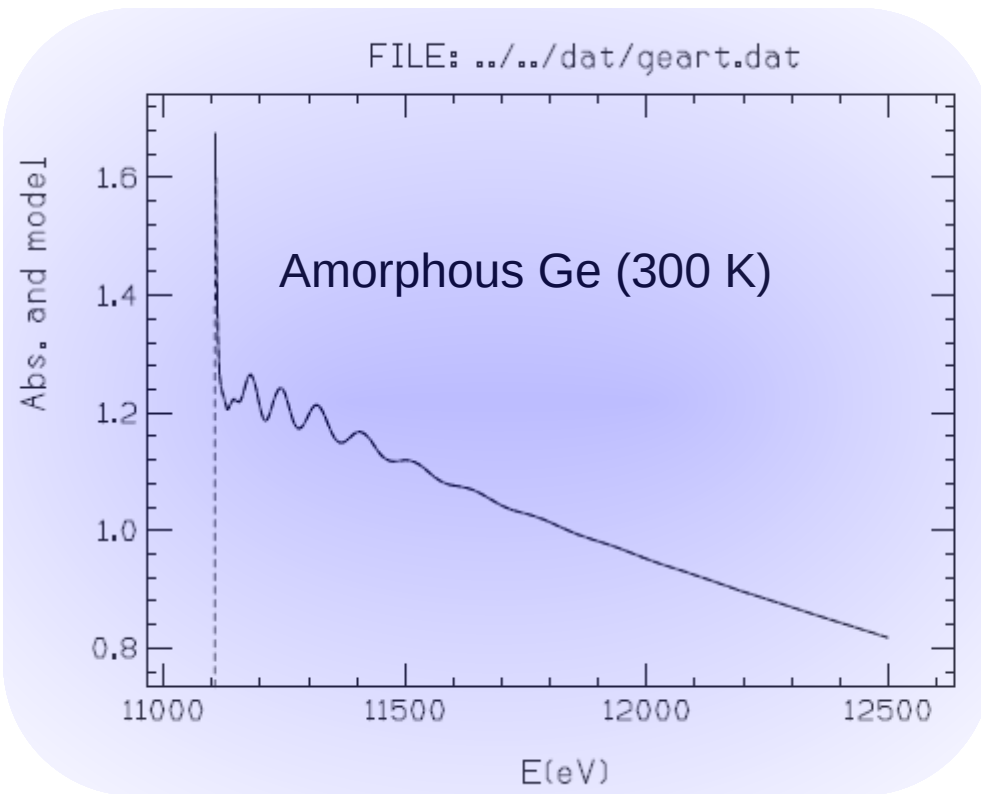
$$W(E_j) = \frac{N}{N - p} \times \frac{k_j^w}{\sum_i [\alpha_N(E_i)^2] \times k_i^w}$$

where  $k_i (\text{\AA}^{-1}) \sim 0.512\sqrt{(E_i - EE)(\text{eV})}$  and  $p$  is the number of parameters used in the minimization.  $\alpha_N(E_i) = \alpha(E_i) - a - b \times E_i$  is the absorption spectrum obtained removing the pre-edge linear background.

- Under normal conditions the weighting function should mimic the energy dependence of the inverse noise variance  $1/\sigma_i^2$ , so that the  $R$  function becomes a standard  $\chi^2$  like statistical function. This can be achieved by tuning the  $w$  (usually 1 – 4) parameter until a satisfactory agreement with the estimated noise is obtained, as can be verified graphically.

# Statistical analysis: noise

- Larger  $w$  values have the effect of giving a larger weight to higher energy data, and this choice can be adopted to reduce the weight of low energy data where the theoretical model may be less accurate.
- The expected value for the residual function  $R$  represents a weighted average squared noise (usually in the range  $10^{-06}$ – $10^{-08}$ ). In most of the real situations the actual minimum value of the residual will exceed these limiting values due to the presence of unexplained signal contributions.



Phys. Rev. B 53, 6174 (1996)

# Statistical analysis

The residual function  $R$  follows the  $\chi_N^2$  distribution, provided that the weight  $W(E_i)$  is proportional to the inverse of the variance  $\sigma^2$  of the  $[\alpha(E_i) - \alpha_m(E_i)]$  random variable. Under these conditions, a full statistical evaluation of the results can be performed:

- 1) *within a given choice for the structural model, the optimal values for the  $\{\lambda\}$  structural parameters are the set  $\{\lambda_{\min}\}$  such that the residual  $R$  is at a minimum.*
- 2) *The statistical  $\chi^2$  test can be performed to check whether the actual value of  $R$  is only due to residual noise or it contains unexplained physical information.*
- 3) *A comparison between two models containing a different number of structural parameters can be performed on the basis of the  $F$ -test, applicable on  $\chi^2$  distributions. For instance, it can be verified if the reduction of  $R$  obtained using more parameters is statistically significant.*
- 4) *Statistical errors related to selected confidence intervals can be estimated for the structural parameters, looking at regions in the parameter space for which  $R(\{\lambda\}) < R_{\min} + C$ , where  $C$  depends on the confidence level chosen and  $R_{\min}$  corresponds to the expected value (when the residual contains only statistical noise). These regions, in the second-order approximation, are  $p$ -dimensional ellipsoids which provide also an insight onto the correlation among parameters.  $R(\{\lambda\})$ , for different realizations of the experimental noise, follows a  $\chi_p^2$  distribution where  $p$  is the number of parameters (see for example pages 684-694 in “Numerical Recipes in Fortran 77”. The value for  $C$  related to a 95% confidence level can be then approximated by  $C \sim R_{\min} \times [p + 2\sqrt{(2p)}] / N$ .*

# Examples of (standard) modern EXAFS data-analysis

The backbone of the GNXAS package is composed of three main codes, in the logical sequence they are:

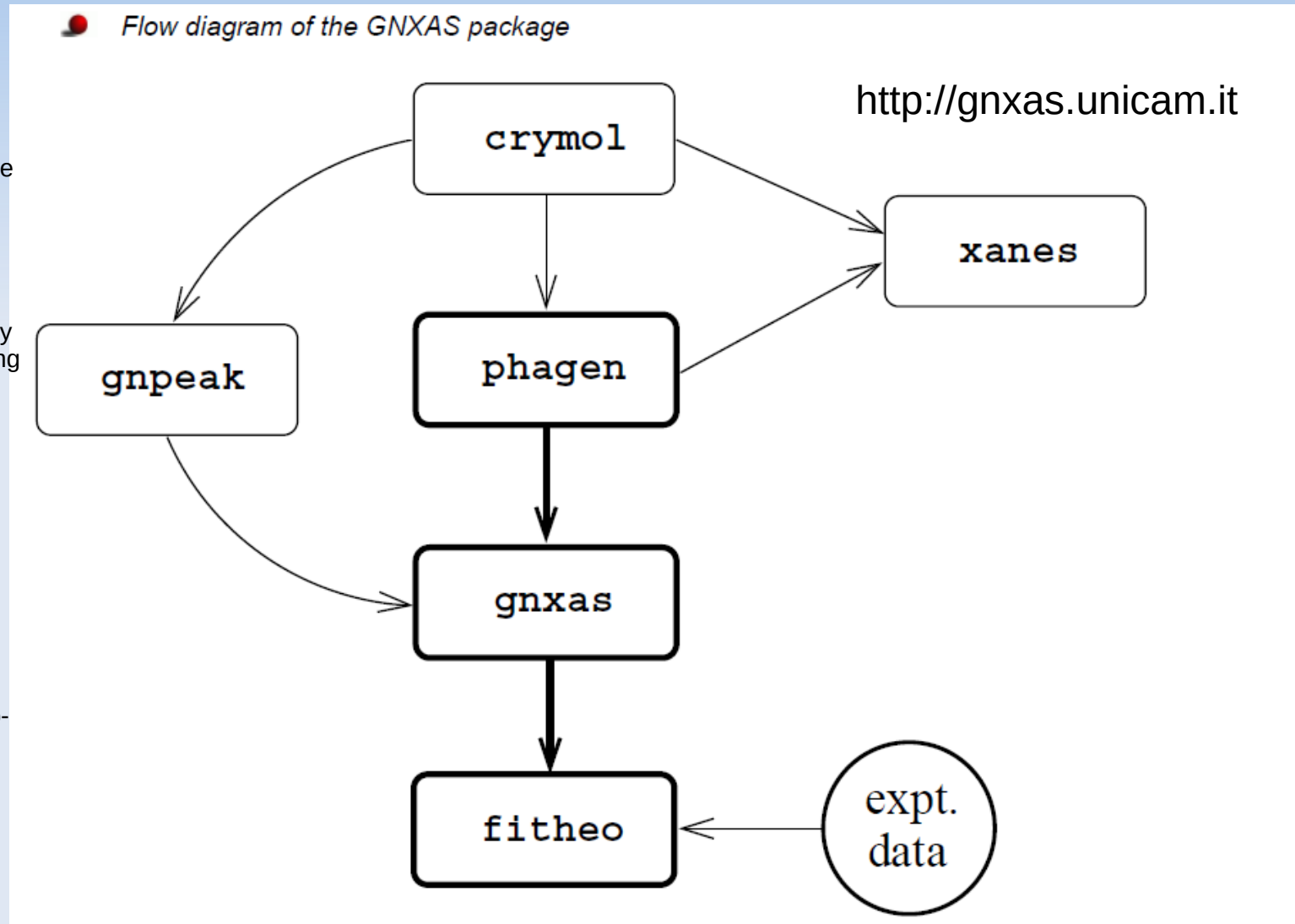
- 1) PHAGEN, potential and phase shift generation.
- 2) GNXAS, signal calculation for reference geometries
- 3) FITHEO, advanced fitting of raw experimental data

Two other programs prepare automatically the input for PHAGEN and GNXAS starting directly from model molecular position or crystallographic data.

4) CRYMOL, allows to treat complex molecular and crystallographic structures providing input information for PHAGEN, GNPEAK, and XANES; the program identifies prototypical phase-shift atoms and select a suitable cluster of atoms for successive XAS calculations.

5) GNPEAK, is based on a general algorithm able to identify inequivalent two-body, three-body and four-body configurations in specified atomic aggregates.

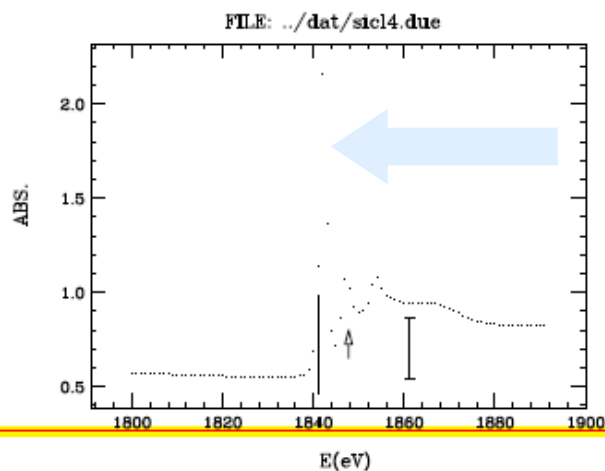
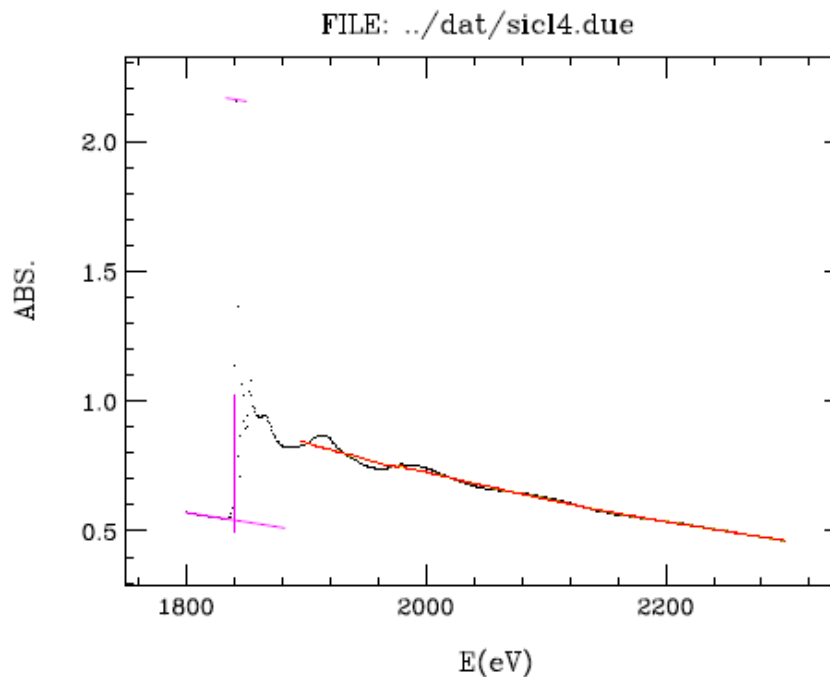
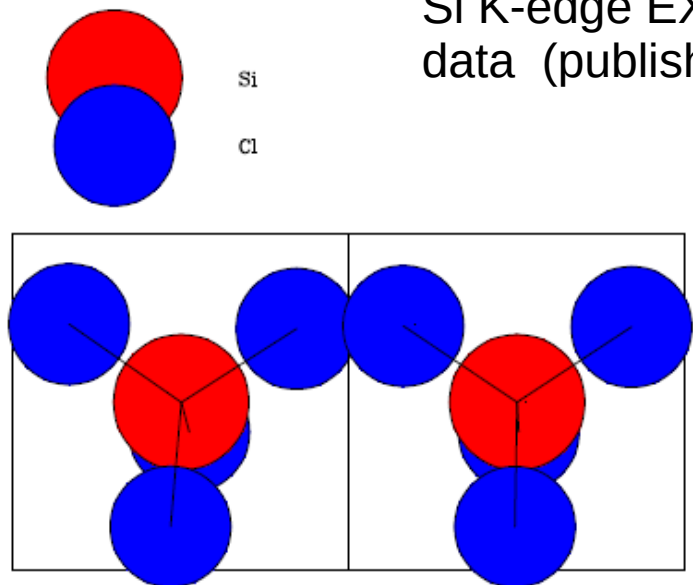
The current distribution includes several other utility programs and versions for Linux, Mac OS, Windows, as well as a graphical interface w-GnXAS.



# Example: gas-phase SiCl<sub>4</sub>

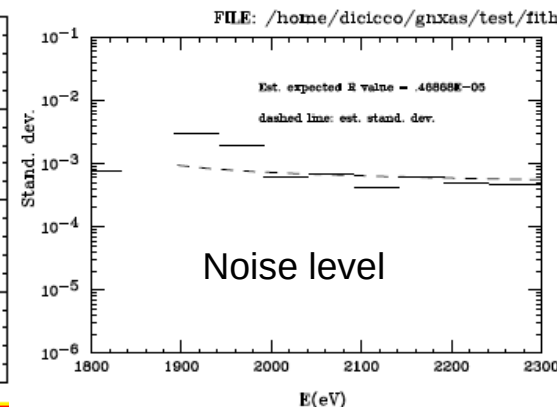
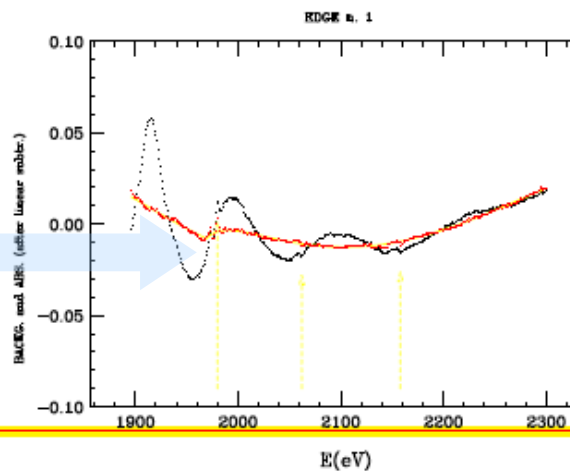
A "classic example": the SiCl<sub>4</sub> gas-phase tetrahedral molecule

Si K-edge EXAFS data (published 1992)



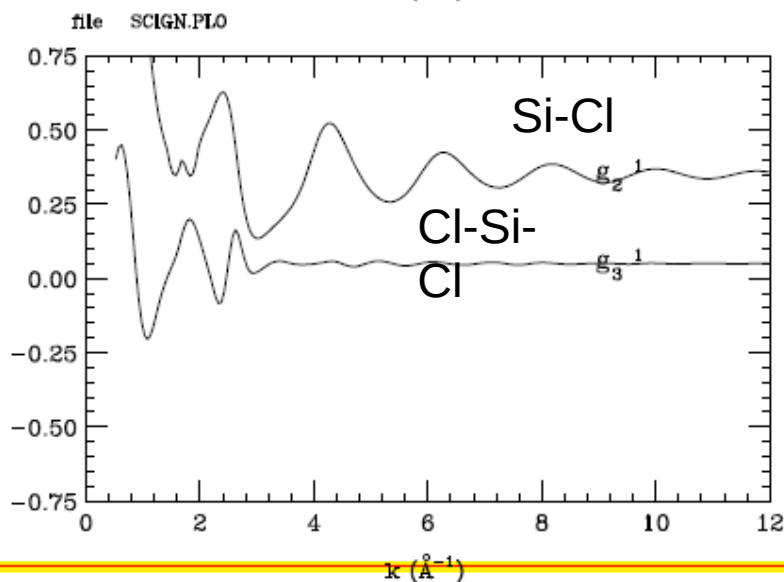
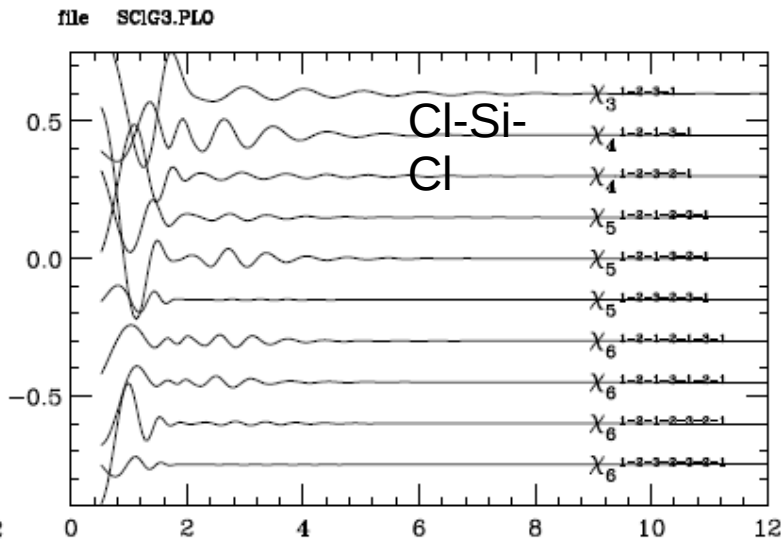
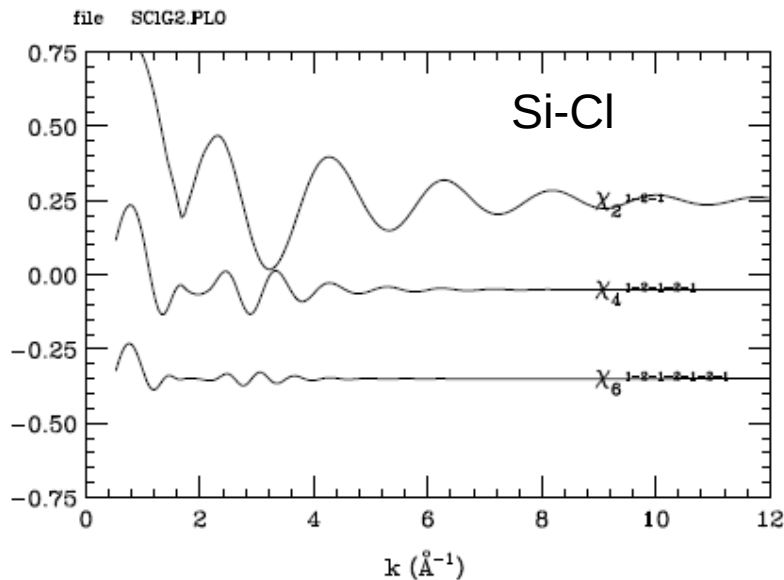
Resonances and molecular bound states in the XANES

1s2p double-electron doublet channel (~1%)



# SiCl<sub>4</sub> – XAS signals

● Calculation of  $\chi$  and  $\gamma$  signals for the SiCl<sub>4</sub> molecule



$$\chi(k) = \sum \chi_2 + \sum \chi_3 + \sum \chi_4 + \dots$$

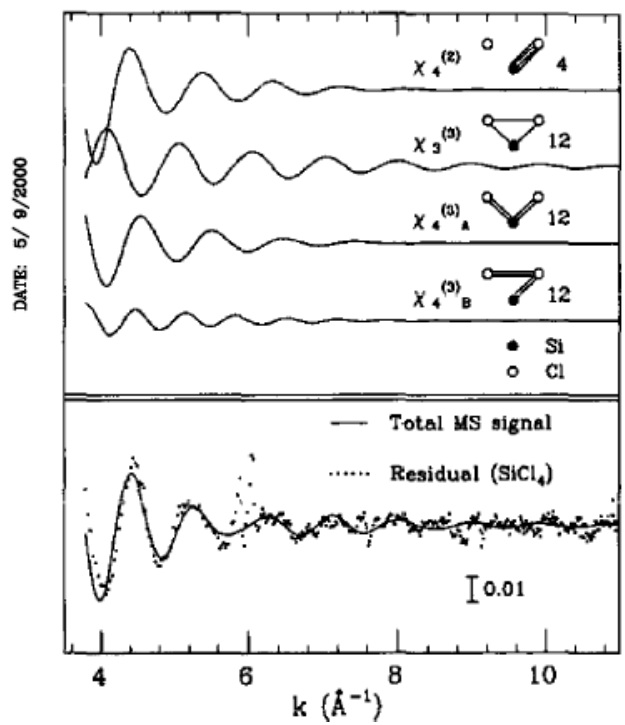
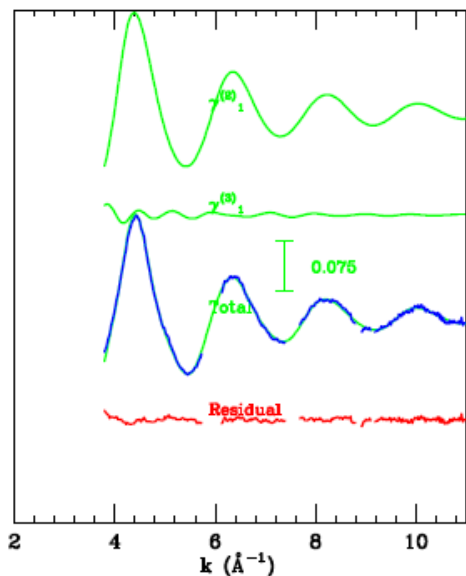
$$\chi(k) = \sum \gamma^{(2)} + \sum \gamma^{(3)} + \sum \gamma^{(4)} + \dots$$

- \* Si-Cl and Cl-Si-Cl multiple-scattering signals ( $\chi_n$ ) calculated for this molecular configuration
- \* Two-body Si-Cl ( $\gamma^{(2)}$ ) and three-body ( $\gamma^{(3)}$ ) Cl-Si-Cl signals for the same molecule
- \* Multiple-scattering and three-body contributions are clearly visible.

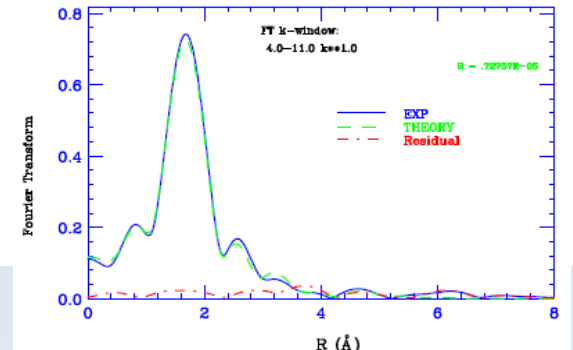
# GnXAS-EXAFS structural results

GNXAS results ( $\text{SiCl}_4$  molecule, A. D. C. et al. *J. Phys. A* 25, 2309 (1992))

FILE: /home/dicicco/gnss/ftmk/fthmo/\_/ftmk/ft  
 NPT: 500 points, 12 parameters, 1 pt, 1 gb, 0 gb  
 Energy range 1800.0 2000.0 weight \*\* 1.0  
 R = .72757E-05



SiCl <sub>4</sub>		
R (Å)	EXAFS	2.021 (8)
R (Å)	Diffraction	2.0193 (34)
σ <sup>2</sup> (10 <sup>-3</sup> Å <sup>2</sup> )	EXAFS	1.5 (3)



- Good agreement with electron diffraction data (in tetrahedral Si-based molecules)
- Need of account for important double-electron 1s2p channels
- Multiple-scattering is observed also in this open structure
- Fourier transform is not useful

# Angle-dependence of MS effects

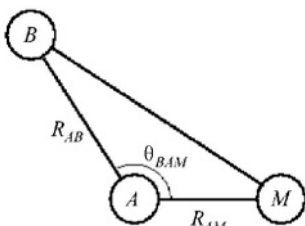


**Figure 1**  
Coordinates of a triangular atomic configuration used for MS simulations.

→ MS in molecules and crystals are always important and become dominant for scattering angles larger than 150 degs

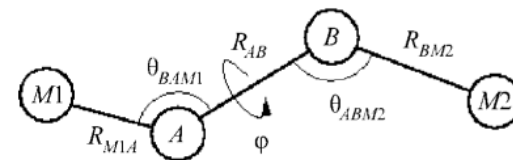


**Figure 3**  
Coordinates of a four-body chain-like molecular fragment used for MS simulations.

MS simulations for molecular fragments relevant for metal biomolecules (Fe-O-O, Fe-CN-Cu) show that 3 and 4-body amplitudes largely exceeds two-body signals near extremal angles → measuring bond angles in complex substances!

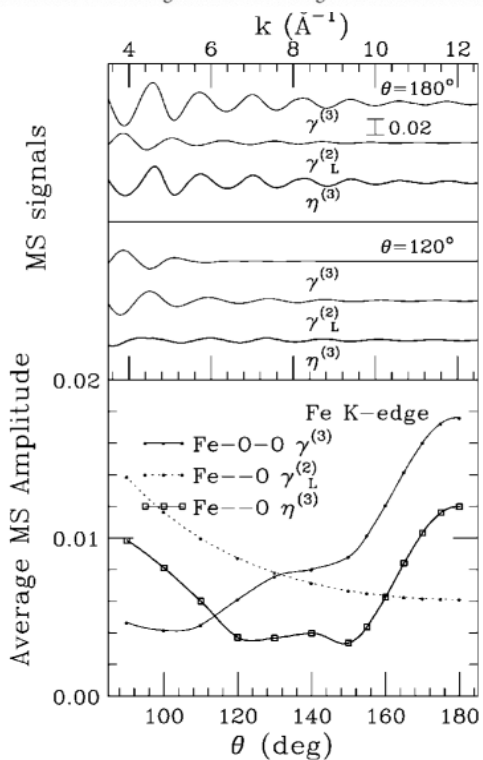


**Figure 2**  
Upper panel: Fe K-edge irreducible  $\gamma^{(2)}$  and  $\gamma^{(3)}$  [ $\eta^{(3)} = \gamma_L^{(2)} + \gamma^{(3)}$ ] MS signals calculated for  $\theta = 180^\circ$  (upper) and  $120^\circ$  (lower) Fe-O-O configurations. Lower panel: average amplitude of the  $\gamma_L^{(2)}$  (dots, Fe-O),  $\gamma^{(3)}$  (solid) and  $\eta^{(3)}$  (squares) MS signals as a function of the bond angle  $\theta$ .

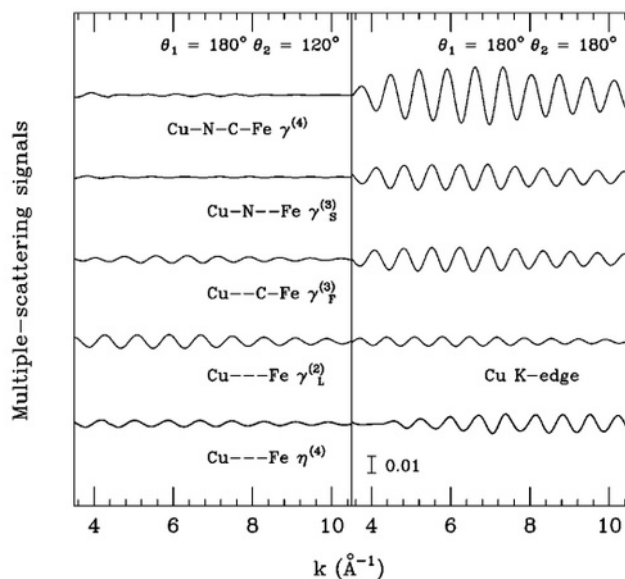


**Figure 4**  
MS irreducible  $\gamma^{(2)}$ ,  $\gamma^{(3)}$  and  $\gamma^{(4)}$  Cu K-edge XAS signals associated with a four-body chain-like Fe-C-N-Cu configuration. The total effective four-body signal  $\eta^{(4)}$  is given by the sum of the  $n$ -body signals involving the fourth atom of the fragment (Fe). The results of the calculations for  $\theta_2 = \theta_{\text{CNCu}} = 120^\circ$  and  $180^\circ$  are reported in the left-hand and right-hand panels, respectively.

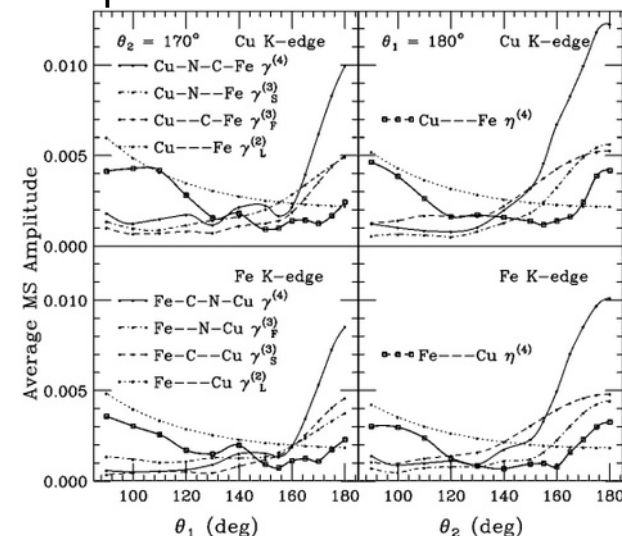


**Figure 5**  
The four panels contain the average amplitudes of the MS signals associated with the four-body Fe-C-N-Cu configuration as a function of the bond angles. Fe and Cu K-edge calculations are reported in the lower and upper panels, respectively. The left-hand panels contain the average amplitudes obtained for fixed  $\theta_2 = 170^\circ$  while the right-hand panels refer to calculations with  $\theta_1 = 180^\circ$ . All of the two-body  $\gamma_L^{(2)}$  (dots), three-body  $\gamma_F^{(3)}$  and  $\gamma_S^{(3)}$  (dashed and dot-dashed), four-body  $\gamma^{(4)}$ , and total  $\eta^{(4)}$  (squares) MS signals are reported.



# MS in molecules- an extreme case

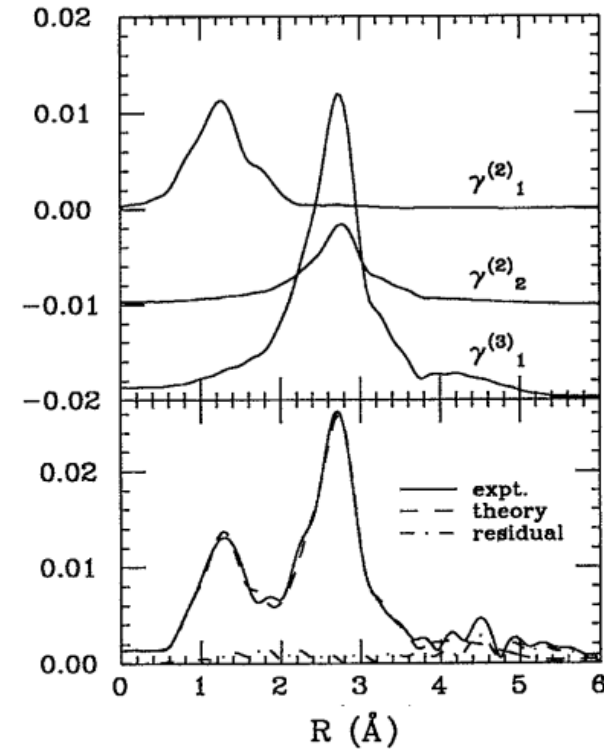
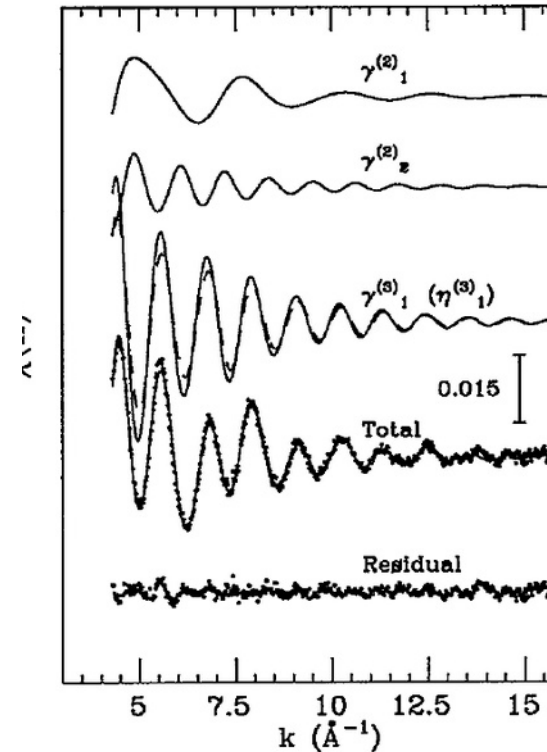
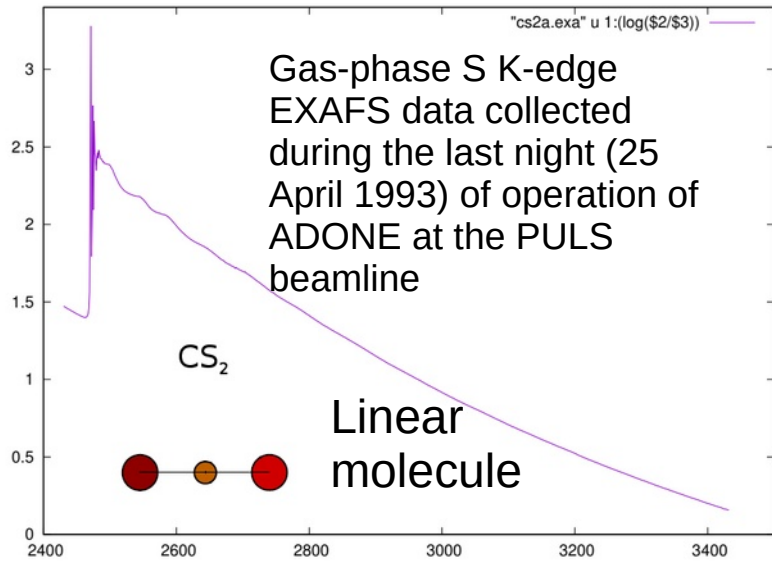
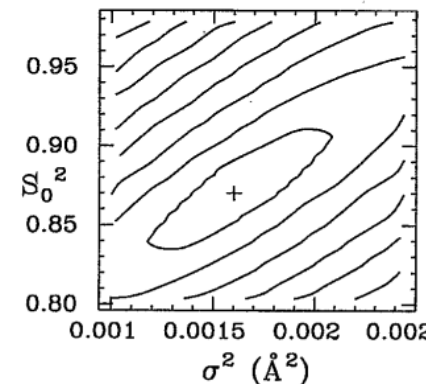


TABLE III. Results of the structural analysis of the CS<sub>2</sub>, S K-edge EXAFS spectrum.

$R$ (Å)	$\sigma^2$ ( $10^{-3}$ Å <sup>2</sup> )	$\delta_\theta^2$ (° <sup>2</sup> )	$\rho_{1,1'}$
1.547(2)	1.6(4)	30(10)	-0.4(2)



→ Good agreement with known electron diffraction data, new info on angle distribution and correlations

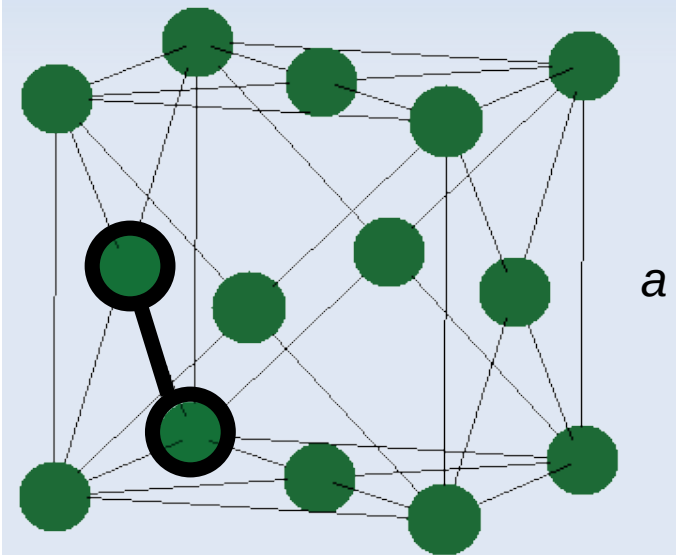
→ Need specialized expressions to treat the extremal case of a collinear three-body distribution (confirmed)

→ Three-body MS is dominant

# Crystals: f.c.c. (1st shell)

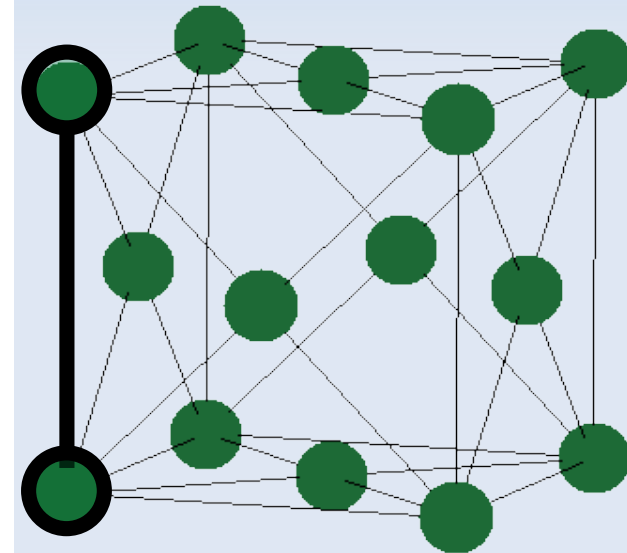
	$R_1/R_0$	$R_2/R_0$	$\Theta$ (deg)	Signal Degeneracy	$R_3/R_0$
$g_2^{(1)}$	1			12	
$g_2^{(2)}$	$\sqrt{2}$			6	
$g_2^{(3)}$	$\sqrt{3}$			24	
$g_2^{(4)}$	2			12	
$g_2^{(5)}$	$\sqrt{5}$			24	
$g_3^{(1)}$	1	1	60	24	1
$g_3^{(2)}$	1	1	90	12	$\sqrt{2}$
$g_3^{(3)}$	1	1	120	24	$\sqrt{3}$
$g_3^{(4)}$	1	1	180	6	2
$g_3^{(5)}$	1	$\sqrt{2}$	90	24	$\sqrt{3}$
$g_3^{(6)}$	1	$\sqrt{3}$	73.22	48	$\sqrt{3}$
$g_3^{(7)}$	1	$\sqrt{2}$	135	24	$\sqrt{5}$

$R_1, \sigma_1^2, \beta_1$   
 $N_1$  (fixed to 12)



# Crystals: f.c.c. (2nd shell)

	$R_1/R_0$	$R_2/R_0$	$\Theta$ (deg)	Signal Degeneracy	$R_3/R_0$
$g_2^{(1)}$	1			12	
$g_2^{(2)}$	$\sqrt{2}$			6	
$g_2^{(3)}$	$\sqrt{3}$			24	
$g_2^{(4)}$	2			12	
$g_2^{(5)}$	$\sqrt{5}$			24	
$g_3^{(1)}$	1	1	60	24	1
$g_3^{(2)}$	1	1	90	12	$\sqrt{2}$
$g_3^{(3)}$	1	1	120	24	$\sqrt{3}$
$g_3^{(4)}$	1	1	180	6	2
$g_3^{(5)}$	1	$\sqrt{2}$	90	24	$\sqrt{3}$
$g_3^{(6)}$	1	$\sqrt{3}$	73.22	48	$\sqrt{3}$
$g_3^{(7)}$	1	$\sqrt{2}$	135	24	$\sqrt{5}$



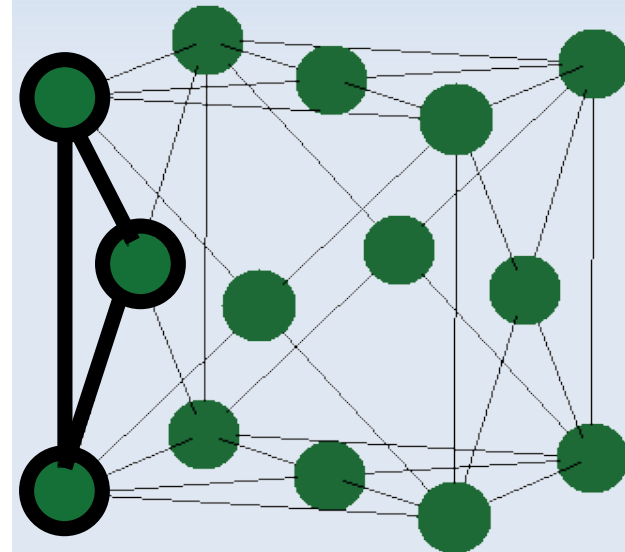
# Crystals: f.c.c. (2nd shell)

	$R_1/R_0$	$R_2/R_0$	$\Theta$ (deg)	Signal Degeneracy	$R_3/R_0$
$g_2^{(1)}$	1			12	
$g_2^{(2)}$	$\sqrt{2}$			6	
$g_2^{(3)}$	$\sqrt{3}$			24	
$g_2^{(4)}$	2			12	
$g_2^{(5)}$	$\sqrt{5}$			24	
$g_3^{(1)}$	1	1	60	24	1
$g_3^{(2)}$	1	1	90	12	$\sqrt{2}$
$g_3^{(3)}$	1	1	120	24	$\sqrt{3}$
$g_3^{(4)}$	1	1	180	6	2
$g_3^{(5)}$	1	$\sqrt{2}$	90	24	$\sqrt{3}$
$g_3^{(6)}$	1	$\sqrt{3}$	73.22	48	$\sqrt{3}$
$g_3^{(7)}$	1	$\sqrt{2}$	135	24	$\sqrt{5}$

new

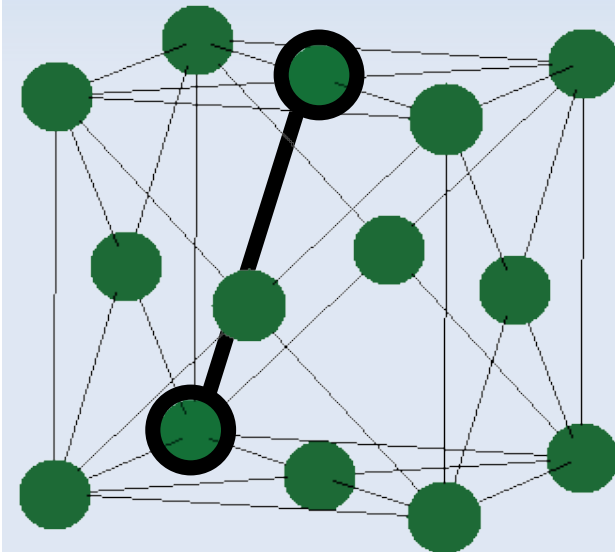
$$\sigma_{R_1 R''_1}, \sigma_{R_1 \Theta_{90}}, \sigma_{\Theta_{90}}, \Theta_{90}^f$$

$N_2$  (fixed to 6)



# f.c.c.: third shell

	$R_1/R_0$	$R_2/R_0$	$\Theta$ (deg)	Signal Degeneracy	$R_3/R_0$
$g_2^{(1)}$	1			12	
$g_2^{(2)}$	$\sqrt{2}$			6	
$g_2^{(3)}$	$\sqrt{3}$			24	
$g_2^{(4)}$	2			12	
$g_2^{(5)}$	$\sqrt{5}$			24	
$g_3^{(1)}$	1	1	60	24	1
$g_3^{(2)}$	1	1	90	12	$\sqrt{2}$
$g_3^{(3)}$	1	1	120	24	$\sqrt{3}$
$g_3^{(4)}$	1	1	180	6	2
$g_3^{(5)}$	1	$\sqrt{2}$	90	24	$\sqrt{3}$
$g_3^{(6)}$	1	$\sqrt{3}$	73.22	48	$\sqrt{3}$
$g_3^{(7)}$	1	$\sqrt{2}$	135	24	$\sqrt{5}$



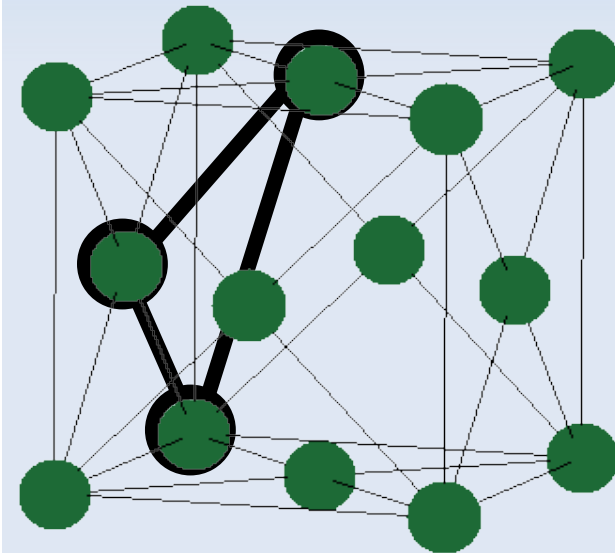
# f.c.c.: third shell

	$R_1/R_0$	$R_2/R_0$	$\Theta$ (deg)	Signal Degeneracy	$R_3/R_0$
$g_2^{(1)}$	1			12	
$g_2^{(2)}$	$\sqrt{2}$			6	
$g_2^{(3)}$	$\sqrt{3}$			24	
$g_2^{(4)}$	2			12	
$g_2^{(5)}$	$\sqrt{5}$			24	
$g_3^{(1)}$	1	1	60	24	1
$g_3^{(2)}$	1	1	90	12	$\sqrt{2}$
$g_3^{(3)}$	1	1	120	24	$\sqrt{3}$
$g_3^{(4)}$	1	1	180	6	2
$g_3^{(5)}$	1	$\sqrt{2}$	90	24	$\sqrt{3}$
$g_3^{(6)}$	1	$\sqrt{3}$	73.22	48	$\sqrt{3}$
$g_3^{(7)}$	1	$\sqrt{2}$	135	24	$\sqrt{5}$

new

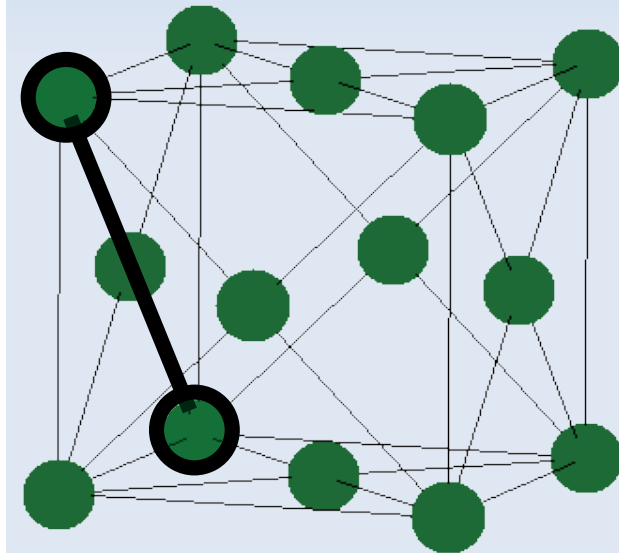
$$\sigma_{R_1 R''_1}, \sigma_{R_1 \Theta_{120}}, \sigma_{\Theta_{120}}, \Theta_{120}^f$$

$$N_3 \text{ (for f.c.c. = } 2N_1)$$



# f.c.c.: fourth shell

	$R_1/R_0$	$R_2/R_0$	$\Theta$ (deg)	Signal Degeneracy	$R_3/R_0$
$g_2^{(1)}$	1			12	
$g_2^{(2)}$	$\sqrt{2}$			6	
$g_2^{(3)}$	$\sqrt{3}$			24	
$g_2^{(4)}$	2			12	
$g_2^{(5)}$	$\sqrt{5}$			24	
$g_3^{(1)}$	1	1	60	24	1
$g_3^{(2)}$	1	1	90	12	$\sqrt{2}$
$g_3^{(3)}$	1	1	120	24	$\sqrt{3}$
$g_3^{(4)}$	1	1	180	6	2
$g_3^{(5)}$	1	$\sqrt{2}$	90	24	$\sqrt{3}$
$g_3^{(6)}$	1	$\sqrt{3}$	73.22	48	$\sqrt{3}$
$g_3^{(7)}$	1	$\sqrt{2}$	135	24	$\sqrt{5}$



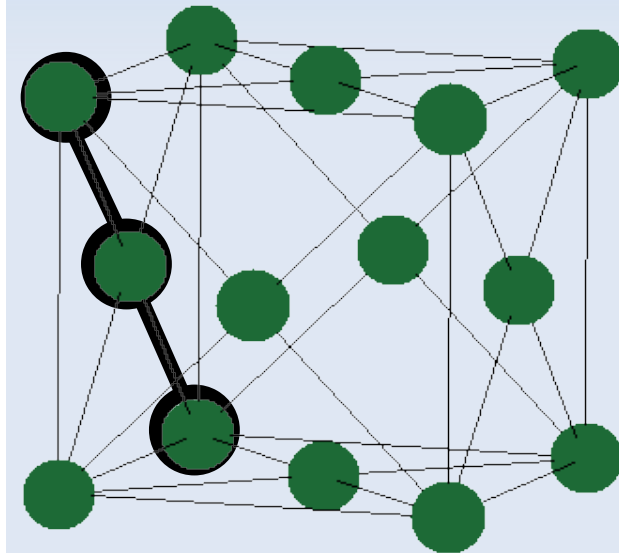
# f.c.c.: collinear configurations

	$R_1/R_0$	$R_2/R_0$	$\Theta$ (deg)	Signal Degeneracy	$R_3/R_0$
$g_2^{(1)}$	1			12	
$g_2^{(2)}$	$\sqrt{2}$			6	
$g_2^{(3)}$	$\sqrt{3}$			24	
$g_2^{(4)}$	2			12	
$g_2^{(5)}$	$\sqrt{5}$			24	
$g_3^{(1)}$	1	1	60	24	1
$g_3^{(2)}$	1	1	90	12	$\sqrt{2}$
$g_3^{(3)}$	1	1	120	24	$\sqrt{3}$
$g_3^{(4)}$	1	1	180	6	2
$g_3^{(5)}$	1	$\sqrt{2}$	90	24	$\sqrt{3}$
$g_3^{(6)}$	1	$\sqrt{3}$	73.22	48	$\sqrt{3}$
$g_3^{(7)}$	1	$\sqrt{2}$	135	24	$\sqrt{5}$

new

$$\sigma_{R_1 R_1^m}, \sigma_{\Theta_{180}}, \Theta_{180}^f$$

$$N_4 \text{ (for f.c.c. = } N_1)$$



Collinear configuration



# Refinement of crystal Pd at 296 K

Two-body (Pd-Pd) and three-body (Pd-Pd-Pd) configurations included up to the 4th neighbors (only 15 parameters, 13 structural + E0 and  $S_0^2$ ).

Very good agreement with crystallographic data and with previously published vibrational amplitudes.

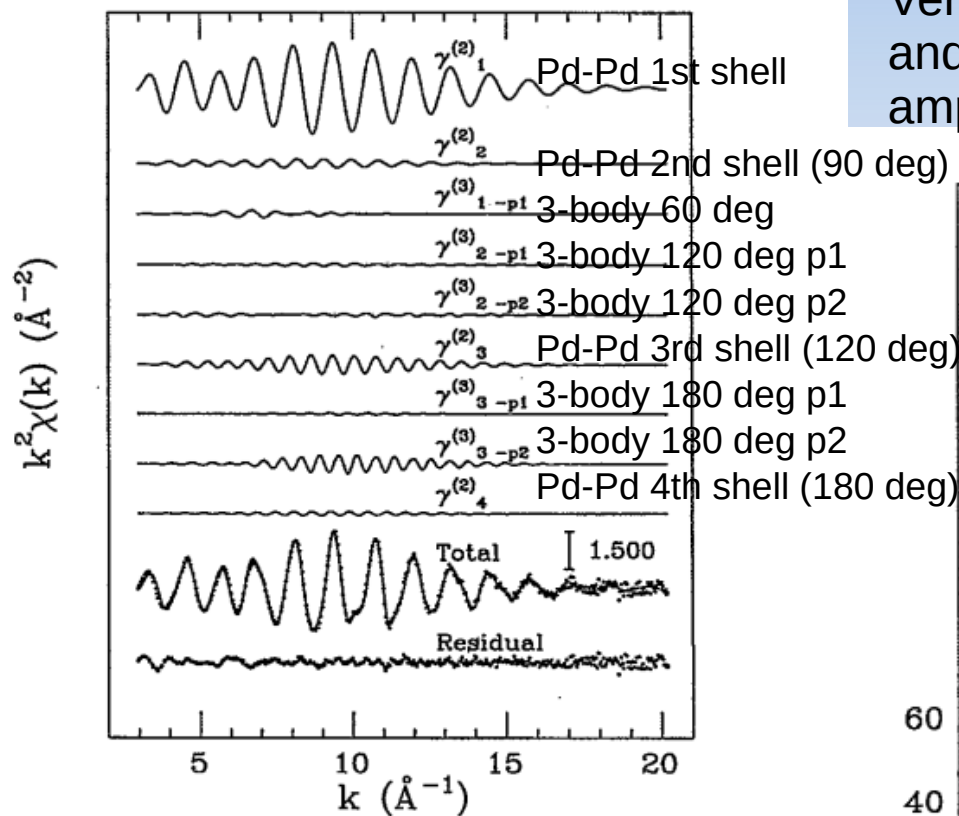


FIG. 8. Best fit of the Pd foil spectrum at 296 K, the various theoretical  $k^2\chi(k)$  signals corresponding to pair and triplet contributions are reported as continuous lines. In the lower part of the figure, the comparison between total theoretical signals (solid line), experiment (dots), and the residual experimental data are reported.

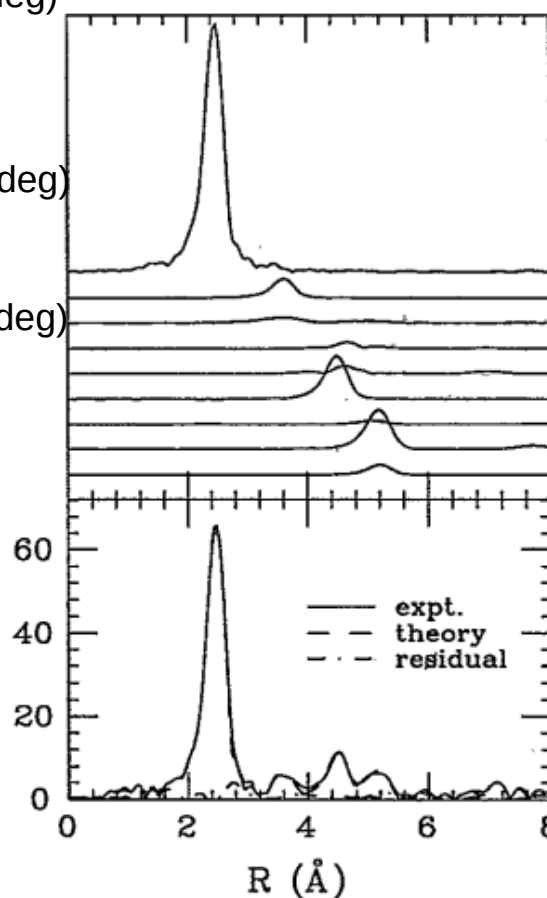
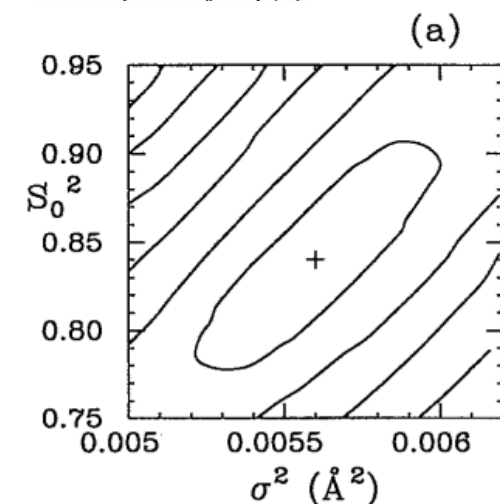


TABLE VII. Results of the structural analysis of Pd foil at 296 K. The parameters for the three triplet configurations correspond to peaks 1, 3, and 4 in Table VI.

Shell	$R$ (Å)	$\sigma^2$ ( $10^{-3}$ Å <sup>2</sup> )	$\beta$
I	2.747(5)	5.6(4)	0.0(1)
II	3.86(2)	10(3)	-1(3)
III <sup>a</sup>	4.77(1)	8.5(10)	
IV <sup>a</sup>	5.49(1)	9.8(10)	
Three-body configurations			
$\theta$ (°)	$\sigma_\theta^2$ (° <sup>2</sup> )	$\rho_{1,1'}$	$\rho_{1,\theta}$
60(f)		$\geq 0.0$	
120.7(4)	$\leq 10$	-0.2(4)	0.0(3)
180(f)	$\leq 10^b$	-0.1(3)	

<sup>a</sup>Derived from the three-body parameters.

<sup>b</sup>Value corresponds to  $\delta_\theta^2$  in Eq. (10).



# Accuracy of XAS structure refinements: crystals

XAS refinements of simple crystalline systems (using MS simulations and peak-fitting) can probe the short-range distribution accurately

- Structural results can enrich the information obtained by XRD/ND.
  - Access to correlated vibrations (related to the phonon density of states)
- XAS provides direct and unique information about the deviation from the harmonic approximation (gaussian distribution of distances)

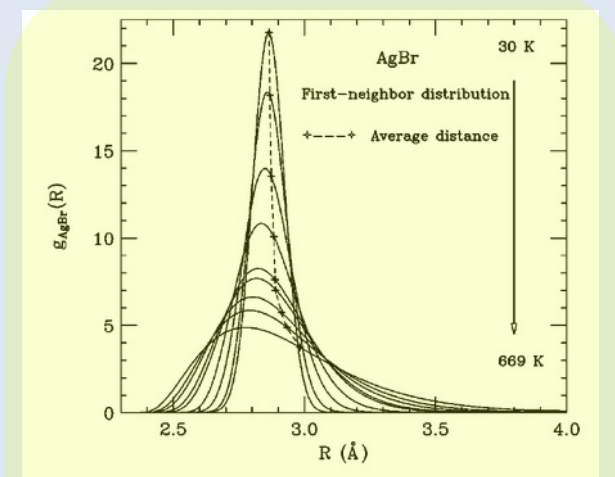
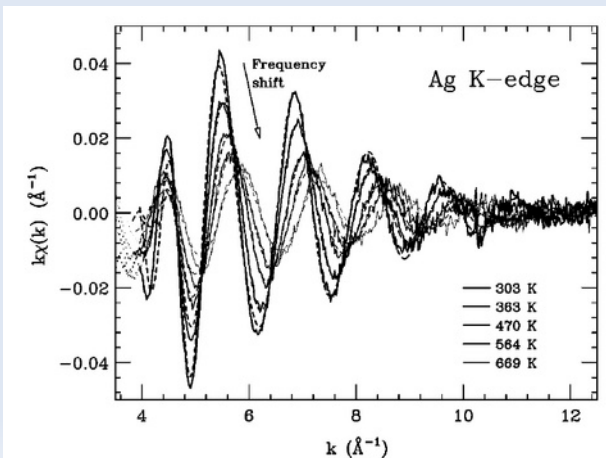
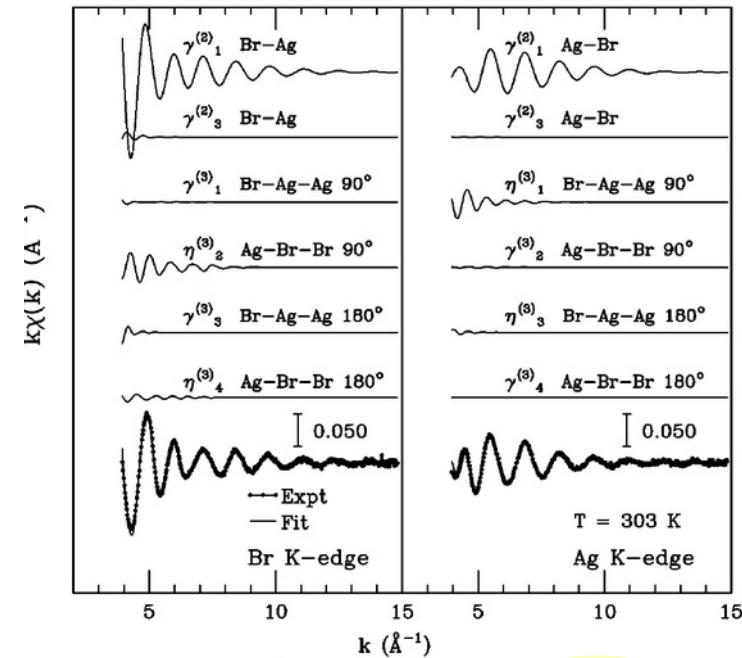
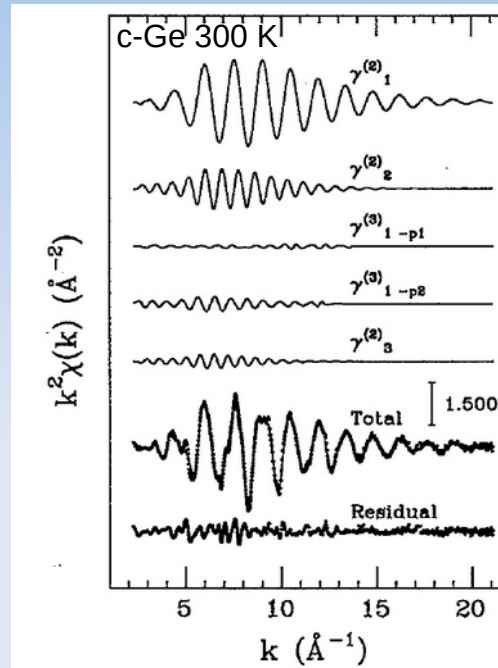
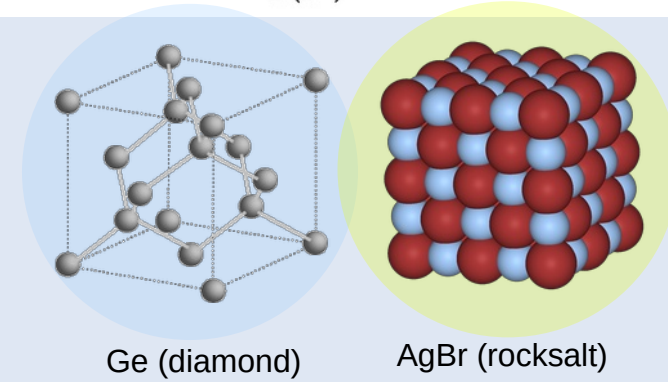


FIG. 10. First-neighbor AgBr distribution as a function of temperature. The average distance increases as a result of the thermal expansion, while the most probable value and the foot of the distribution shift toward shorter distances.



Phys. Rev. B, 62, 12001 (2000)

# XAS particularly useful in disordered matter

## Typical systems:

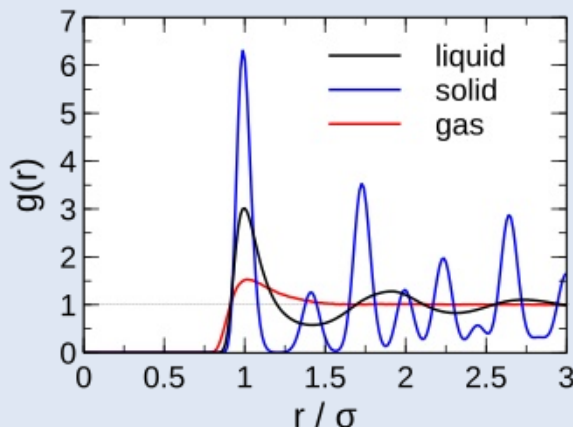
- 1) gases, liquids (thermodynamical equilibrium)
- 2) amorphous solids (including glasses, plastic/polymers, gels)
- 3) disordered thin films/ill-ordered nanostructures/alloys and composites

## Main advantages:

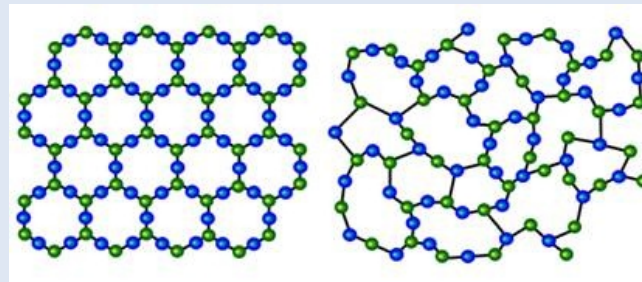
- 1) chemical selectivity
- 2) local probe, highly sensitive to short-range
- 3) experiments accessible under various sample environments
- 4) probing metastable and transient states

Standard experimental techniques for structural studies include x-ray and neutron diffraction, as well as spectroscopies like Raman scattering

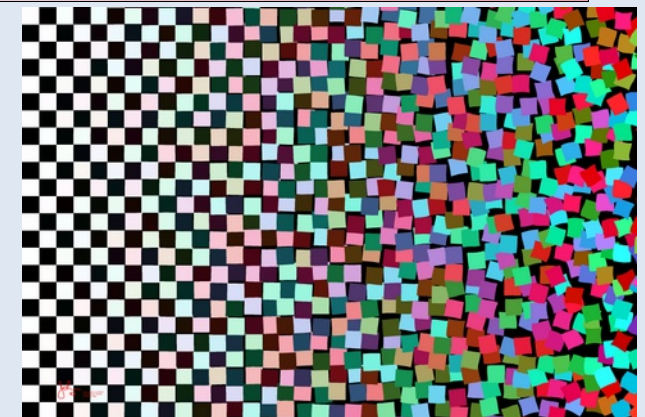
XAS is powerful and highly complementary to the other techniques, but is blind to long-range correlations and needs complex data-analysis



Pair distribution function  $g(r)\rho 4\pi r^2 dr$   $r = dn(r)$



Courtesy [www.bnc.hu](http://www.bnc.hu)



# XAS and atom distributions (disorder)

$$\begin{aligned}
 \langle \chi(k) \rangle = & \int_0^\infty dr 4\pi r^2 \rho g_2(r) \gamma^{(2)}(r, k) + \int dr_1 dr_2 d\phi 8\pi^2 r_1^2 r_2^2 \sin(\phi) \rho^2 g_3(r_1, r_2, \phi) \\
 & \times \gamma^{(3)}(r_1, r_2, \phi, k) + \int dr_1 dr_2 d\phi dr_3 d\Omega 8\pi^2 r_1^2 r_2^2 r_3^2 \sin(\phi) \rho^3 g_4(r_1, r_2, \phi, r_3, \Omega) \\
 & \times \gamma^{(4)}(r_1, r_2, \phi, r_3, \Omega, k) \dots \dots
 \end{aligned}$$

(19)

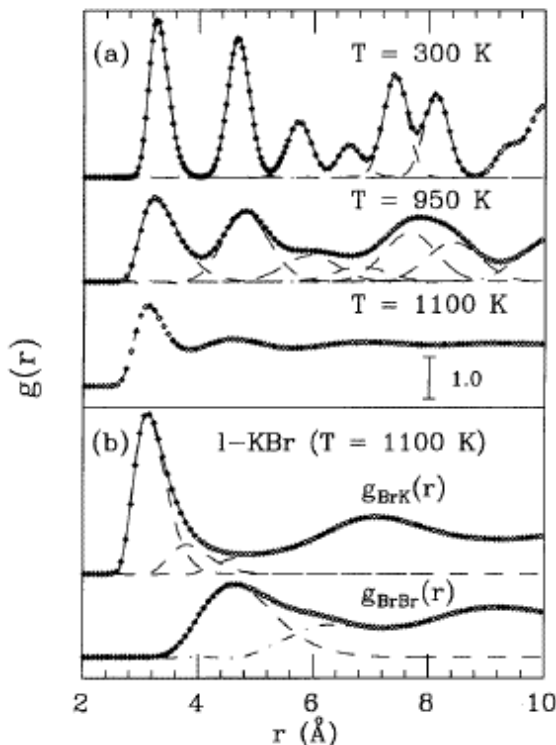
A. Filipponi, A. Di Cicco and C. R. Natoli, Phys. Rev. B 52, 15122 (1995)

Structural refinement of the raw data through MS calculation of the XAS cross section (GNXAS  $\rightarrow \gamma^{(n)}$  signals, corresponding to  $g^{(n)}$  distributions)

- the distance distribution is assumed to be a superposition of distinct peaks ("shells") whose parameters ( $N, R, \sigma^2, \dots$ ) are fitted to the experimental data
- valid also for reconstructing the  $g(r)$  in simple [1] and binary [2] liquids introducing physical constraints accounting for the density and the compressibility of the system

## Needs:

- Extension of the refinement scheme to multi-component systems and higher-order distributions
- Model independent approach
- Simultaneous refinement of short and long-range order (XAS+diffraction)

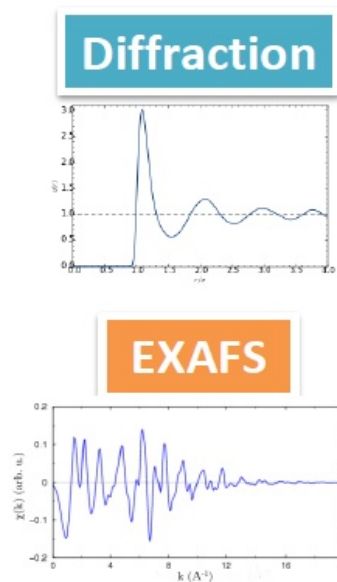


[1] A. Filipponi, Journal of Physics: CM 13, R23 (2001)  
 [2] Angela Trapananti and Andrea Di Cicco, Phys. Rev. B 70, 014101 (2004)

# Beyond the peak-fitting approach

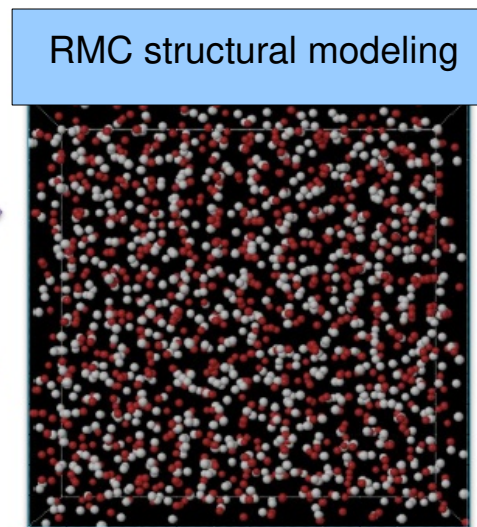
## Data analysis: Reverse Monte Carlo

RMC is structural modelling approach to produce three dimensional atomic models of disordered materials which are consistent with a set of experimental data



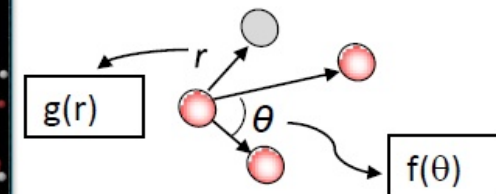
$\chi^2$

Sampling driven by the experimental data



<http://gnxas.unicam.it>

Implemented within the GNXAS package for elemental and multi-atomic systems



$$\chi^2 = \sum_{n=1}^{N_{EDGE}} \sum_{i=1}^{N_{XAS}} \frac{[\gamma_{En}^{(2)}(k_i) - \gamma_{Cn}^{(2)}(k_i)]^2}{\sigma_{n,i}^2} + \sum_{\alpha,\beta} \sum_{j=1}^{N_g} \frac{[g_{\alpha\beta}^E(r_j) - g_{\alpha\beta}^C(r_j)]^2}{\sigma_{\alpha,\beta,j}^2}$$

First refs. on the RMC-GNXAS method (applied to Br<sub>2</sub> and liquid Cu): Phys. Rev. Lett. 91, 135505 (2003) J. Phys. Condens. Matter 17 S135 (2005)

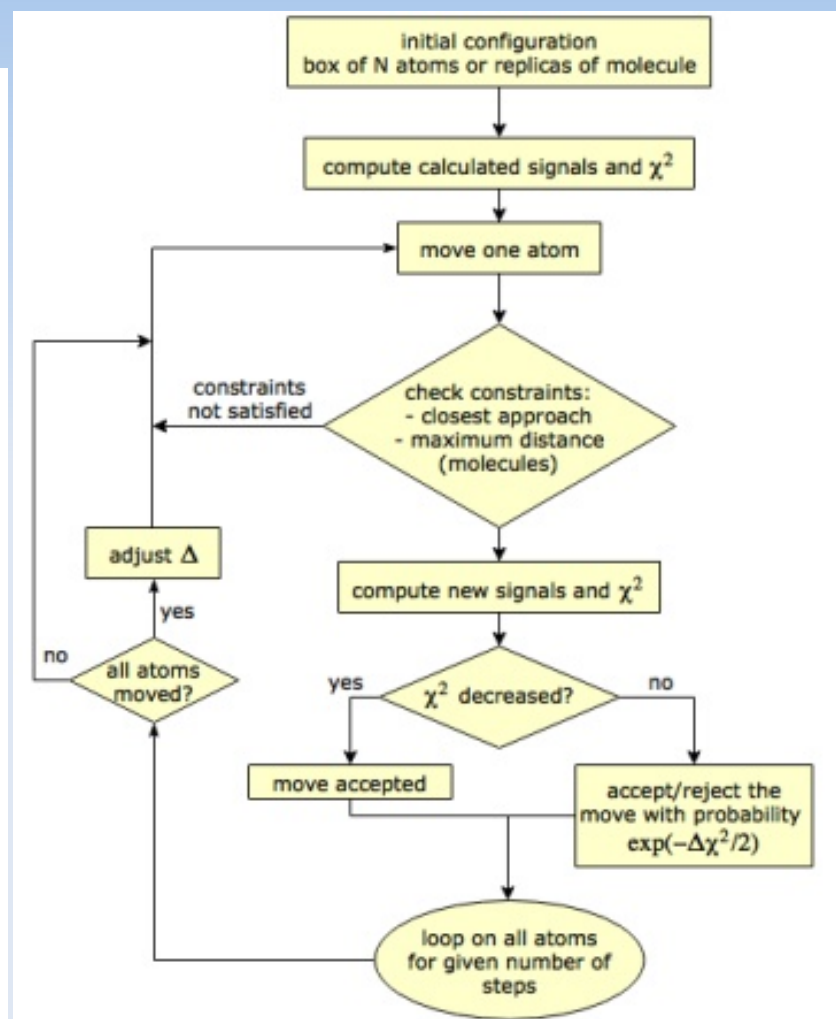
- RMC fully exploits the complementarity of different techniques
- 3d models: structural information beyond the average distance

# RMC-GnXAS implementation

Presently fully implemented for multi-atomic ordered or disordered systems using model pair distributions as a constraint for long-range correlations and density (from XRD, ND, MD, MC ...).

$$\chi^2 = \sum_{n=1}^{N_{\text{EDGE}}} \sum_{i=1}^{N_{\text{XAS}}} \frac{[\chi_n^E(k_i) - \chi_n^C(k_i)]^2}{\sigma_{n,i}^2} + \sum_{\alpha,\beta} \sum_{j=1}^{N_g} \frac{[g_{\alpha\beta}^E(r_j) - g_{\alpha\beta}^C(r_j)]^2}{\sigma_{\alpha\beta,j}^2}$$

- o Atomic displacement  $\Delta$  iteratively modified to have acceptance ratio  $\sim 0.5$
- o Molecular replica or periodic boundary conditions applied
- o For molecules,  $g(r) \rightarrow n(r)$  since the density is not defined



See review paper and refs. therein: A. Di Cicco and F. Iesari, PCCP 24, 6988 (2022).

# Accuracy of RMC-GnXAS: molecules

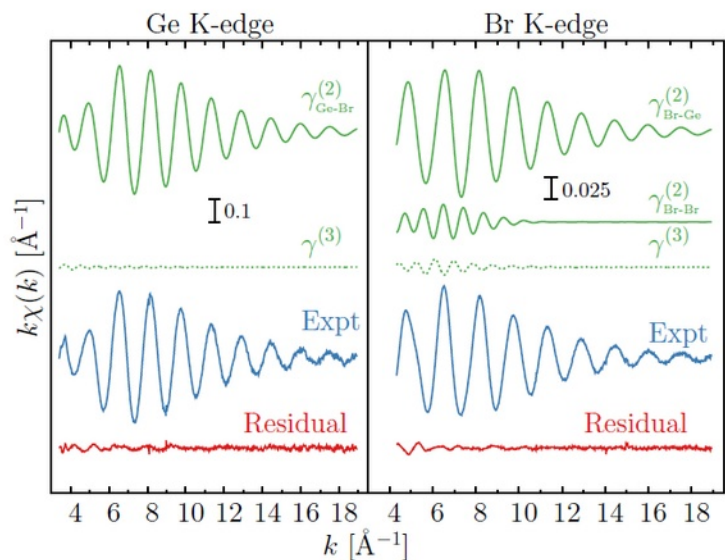
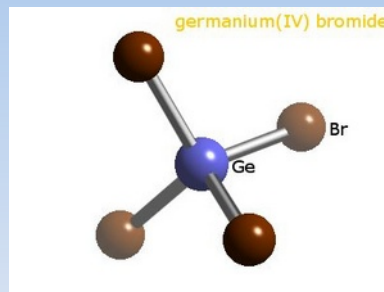
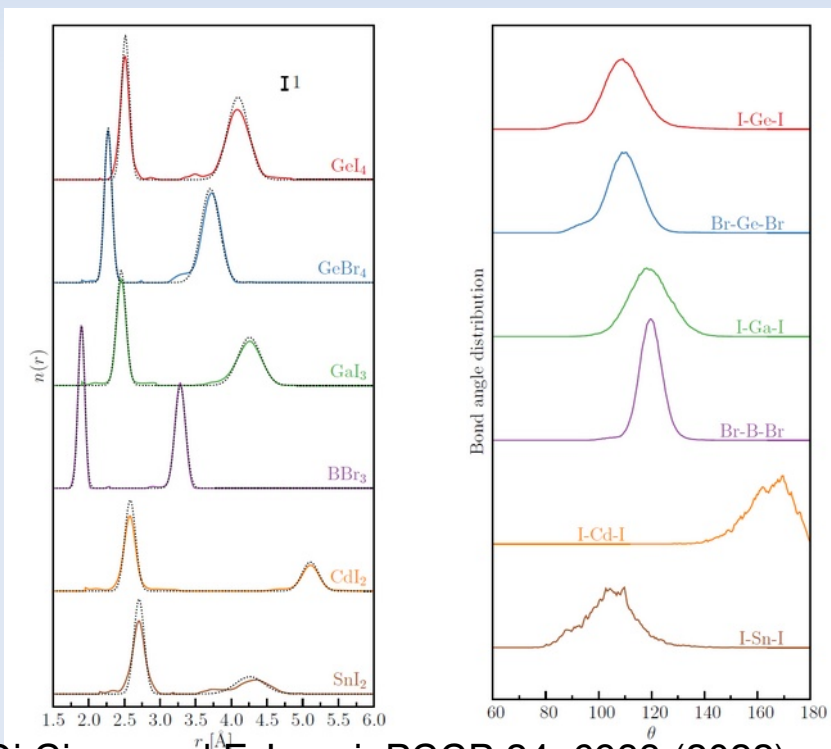


Figure 6. Double-edge RMC refinement of the Ge (left) and Br (right) K-edge EXAFS spectra of the  $\text{GeBr}_4$  gas-phase system (temperature  $T=403$  K). The calculated two-atom EXAFS signals resulting from a set of molecular configurations (green lines) are compared with the corresponding experimental data (blue lines). The weak three-body ( $\gamma^3$ ) signals associated with the Br-Ge-Br triplet configurations are also shown. The residual curves are shown in red color (bottom).



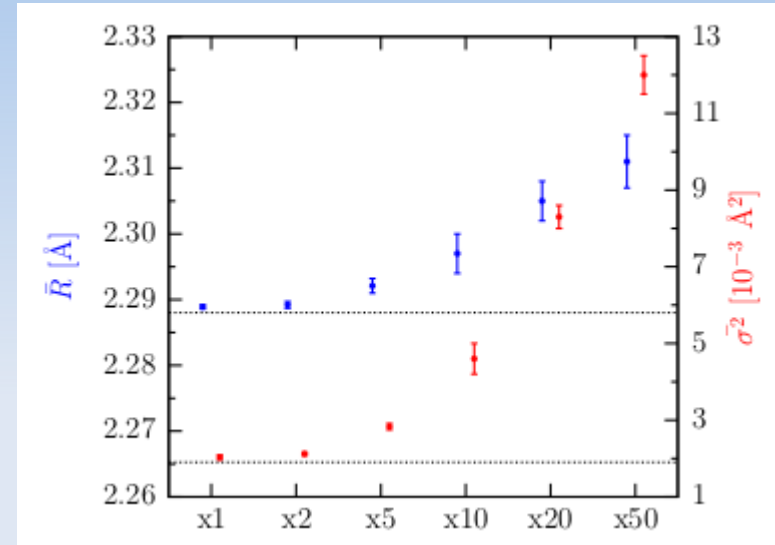
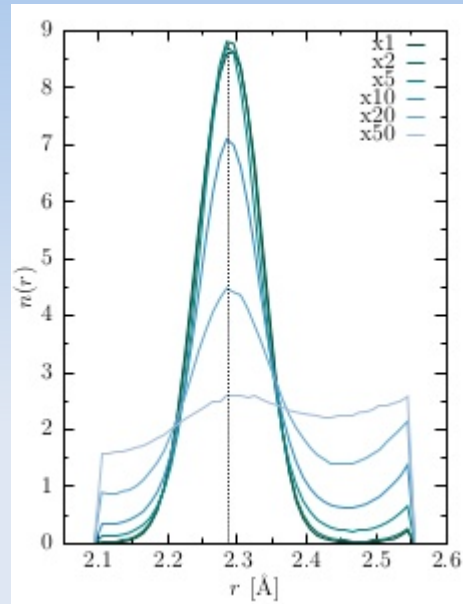
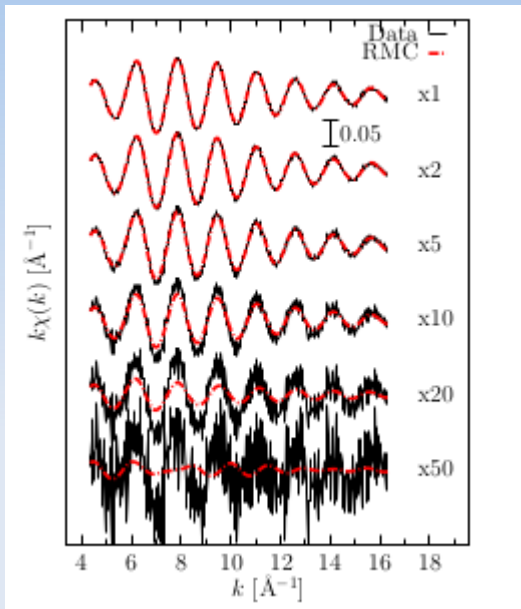
Multiple-edge XAS refinements provide reliable determination of the short-range structure in molecules and condensed matter (using both RMC and peak-fitting techniques)



- Excellent agreement with electron diffraction data
- Reconstruction of radial and bond-angle distributions.

A. Di Cicco et al., J. Chem. Phys. 148, 094307 (2018), A. Di Cicco and F. Iesari, PCCP 24, 6988 (2022).

# Noise and uncertainty on structure refinements by RMC-GnXAS



- o Br<sub>2</sub> (average noise on original XAFS experimental data  $\sim 10^{-6}$ , N/S  $\sim 10^{-5}$ ).
- o Different RMC refinements adding artificial noise (see factors).
- o Deviations and larger error bars observed for increasing noise levels.

Other factors among many contributing to the uncertainty on reconstructed structure:  
1)  $k$  extension of the XAFS data; 2) number and type of data sets (multiple-edge XAFS, partial  $g(r)/n(r)$  distributions obtained by diffraction; 3) number of atoms of the RMC simulation box (roughly of the same order of the data points).



# RMC-GnXAS in crystals: c-Ge

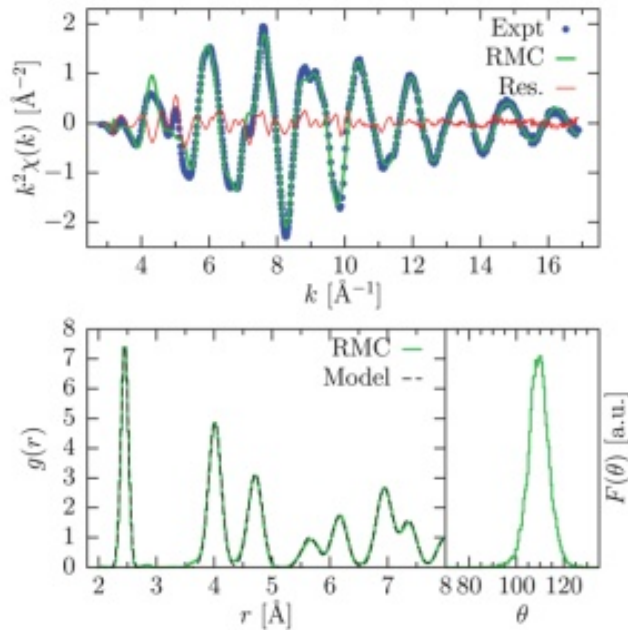


**Fig. 4** Results of the RMC refinement of room temperature crystalline Ge. Upper panel: experimental K-edge XAFS signal (Expt, blue points) compared with the result of the RMC simulation after convergence (RMC, green line). The difference spectrum is also shown (Res., red line). Bottom panels: on the left, the pair distribution function  $g(r)$  resulting from RMC refinement (RMC) is compared with the model used also as a constraint. On the right, the bond-angle distribution of the nearest-neighbors is shown, which shows a clear peak centered around  $109^\circ$ .

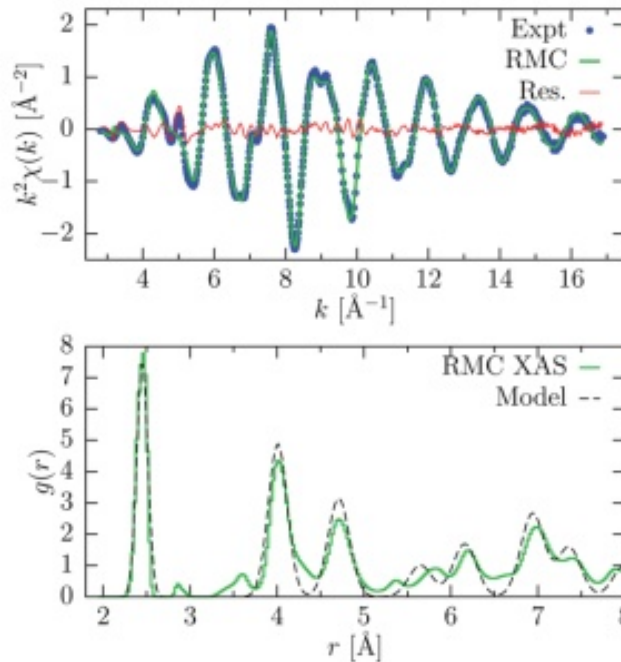


**Fig. 5** Results of the RMC refinement of room temperature crystalline Ge using only XAFS data. Upper panel: experimental K-edge XAFS signal (Expt, blue points) compared with the result of the RMC simulation after convergence (RMC, green line). The difference spectrum is also shown (Res., red line). Bottom panel: the pair distribution function  $g(r)$  resulting from RMC refinement (RMC) is compared with the model shown in the previous figure.

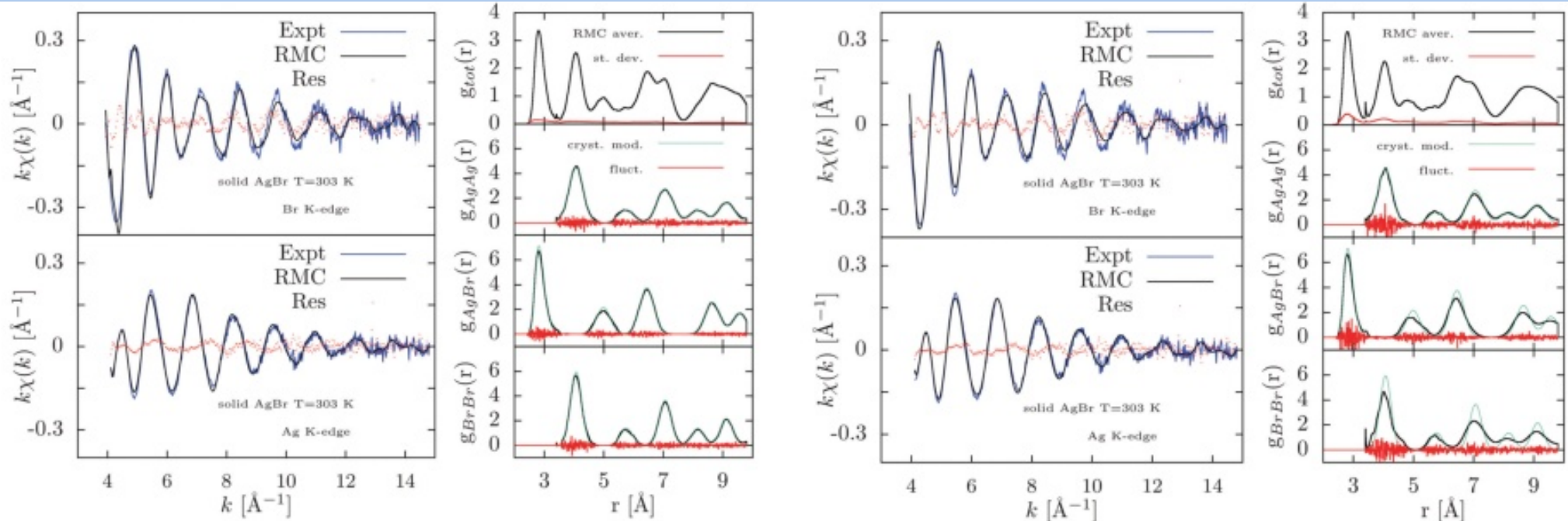
- o Excellent agreement at short-range with diffraction data/models
- o Constraints to the diamond crystal structure with proper vibrational amplitudes necessary beyond the first shell (unphysical features in  $g(r)$  when  $r$  larger than  $\sim 3 \text{ \AA}$ ).

Ensemble of 1728 atoms with periodic boundary conditions,  $6 \times 6 \times 6$  diamond structure f.c.c. cells ( $a=5.658 \text{ \AA}$ ).

[2] A. Di Cicco and F. Iesari, Phys. Chem. Chem. Phys. 24 6988 (2022)

Warning! In crystals correct long-range constraints must be used to retain the crystal structure

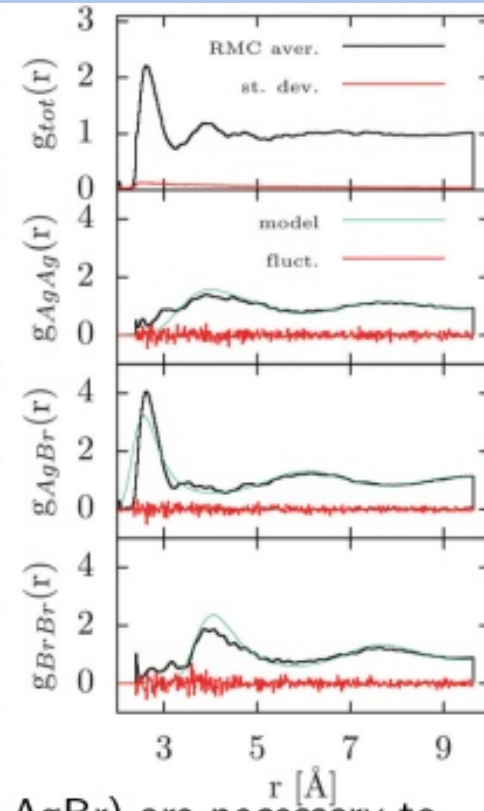
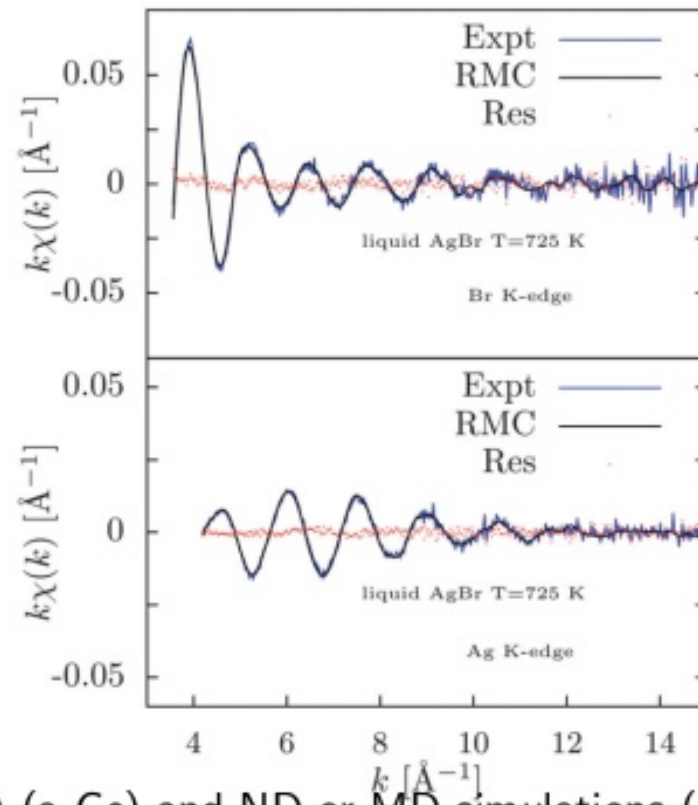
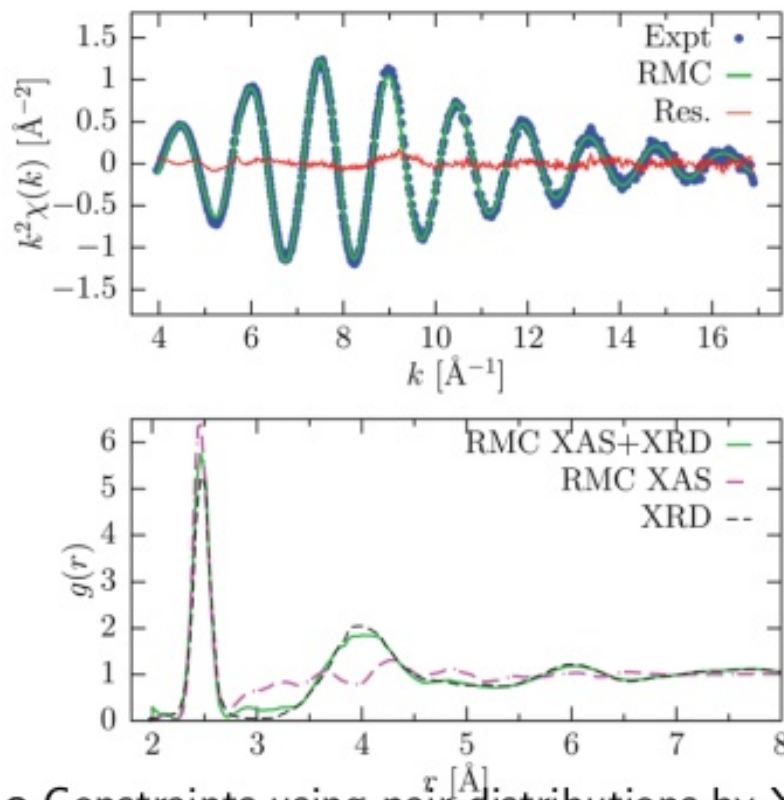
# Multiple-edge RMC-GnXAS on crystals: AgBr



- o RMC refinement including realistic constraints for the medium-range Ag-Br, Ag-Ag, Br-Br structure preserve the crystalline structure and correct vibrational amplitudes
- o The unconstrained XAFS refinement (right-side) show larger fluctuations and broadening of the medium-range peaks.

Ensemble of 1000 atoms with periodic boundary conditions, 5x5x5 f.c.c. cells ( $a=5.7745 \text{ \AA}$ ). [2] A. Di Cicco and F. Iesari, Phys. Chem. Chem. Phys. 24 6988 (2022)

# RMC-GnXas in amorphous and liquid systems



- o Constraints using pair distributions by XRD (a-Ge) and ND or MD simulations (l-AgBr) are necessary to obtain realistic shapes beyond the first-neighbors.
- o The unique XAFS short-range sensitivity allowed us to improve present knowledge of the short-range distributions. [2] A. Di Cicco and F. Iesari, Phys. Chem. Chem. Phys. 24 6988 (2022) for AgBr see also A. Di Cicco et al., Phys. Rev. B, 62, 12001 (2000)

# XAS of elemental liquids

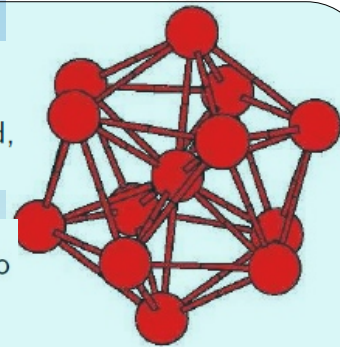
- Elemental liquids represent the simplest example of condensed disordered system under thermodynamical equilibrium.
- Measuring XAS of elemental liquids require solutions for sample design and high temperature conditions (with some notable exceptions like liquid Hg, Ga)
- Advances in experimental techniques allowed us to obtain accurate XAS measurements under controlled high-pressure and temperature conditions
- Phase transitions can be continuously monitored by a combination of techniques
- XAS has unique capabilities for measuring local structure of deeply undercooled liquids

Examples of open problems:

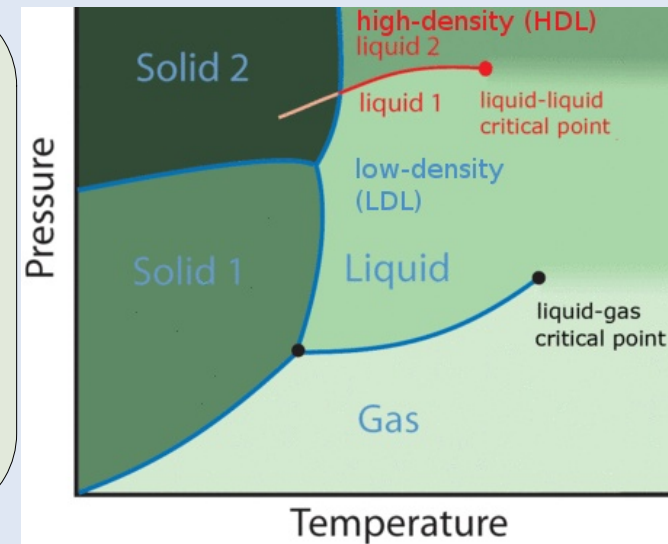
- Icosahedral ordering in close-packed liquids
- Poly(a)morphism of the liquid → existence of liquid-liquid transitions

The old hypothesis [F. C. Frank, Proc. R. Soc. London, Ser. A 215, 43 (1952)] that close packed liquids may develop an icosahedral order, especially when undercooled, has attracted attention for over half a century.

We contributed with a series XAS investigations of undercooled liquid elemental metals (Pd, Cu, Sn, Ni, ...) also addressing the issue of the degree of icosahedral local order developing in the melt.



>Polymorphic substances may show transitions also in their disordered phases (glass, undercooled liquid, liquid)  
>This phenomenon is known to occur for amorphous ice under pressure, and has been suggested in other open-structure amorphous (or deeply undercooled) systems (low-density tetrahedral C, Si, Ge ..)  
>Indications for liquid-liquid transitions in polymorphic metals (for example Sn, Bi) were also obtained by different techniques.



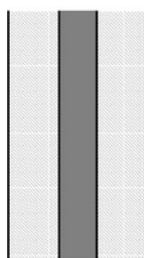
>Our XAS investigations regarded the occurrence of transitions in the Sn, Bi (undercooled) liquids under pressure, as well as in amorphous Ge and chalcogenides

# Sample design and combination of x-ray techniques for measuring liquids

## Techniques:

- ① X-ray absorption spectroscopy (XAS) → *short-range ordering*
- ② X-ray diffraction (angular, energy-scanning) → *medium and long-range ordering*
- ③ Single-energy XAS → *structure transformation/phase transition detection*

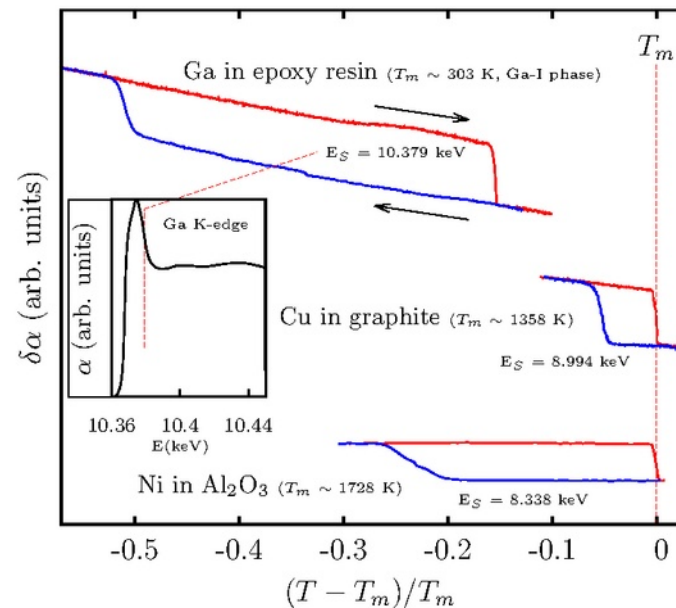
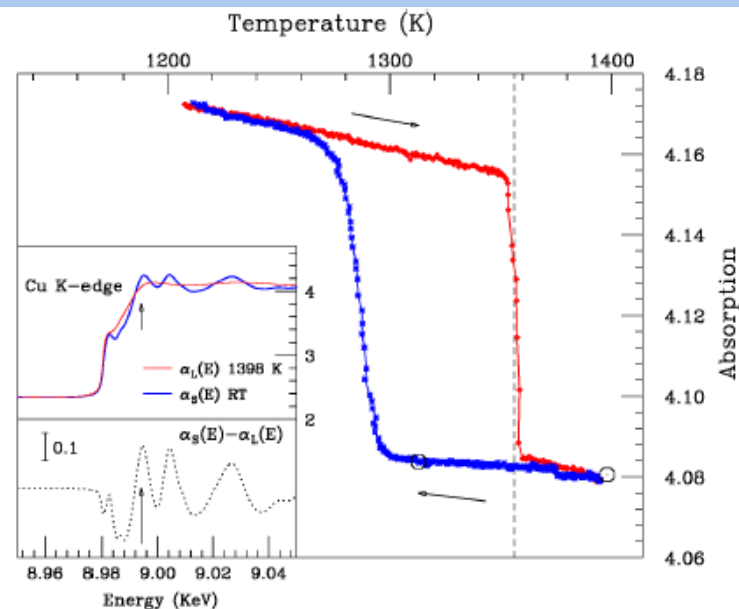
The sample is usually dispersed (b) into a "chemically inert" matrix, low x-ray absorbing and high-temperature resistant (like BN, C,  $\text{Al}_2\text{O}_3$ ,  $\text{ZrO}_2$ ). Micrometric powders of pure materials can be undercooled quite easily hundreds Celsius below the melting point.



(a)

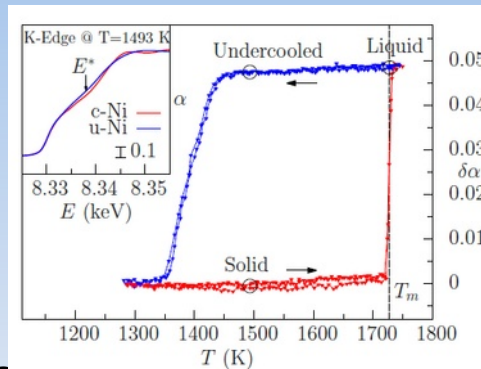


(b)

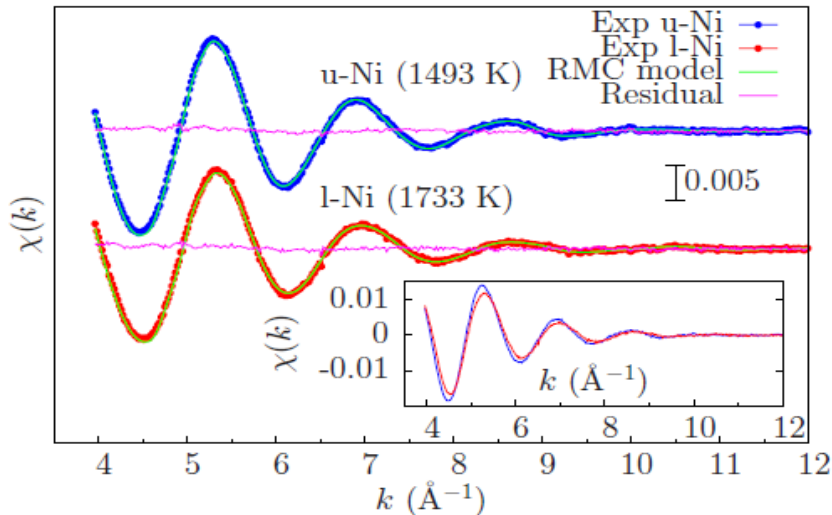


# Liquid Ni: unique insight on liquid structure

Pinning liquid and solid phases at high temperature by single-energy Tscan



High-quality EXAFS spectra, differences among liquids at different temperatures



Refs: J. Phys. Condens. Matter 17 S135 (2005), Physical Review B 89, 060102 (2014)

→ Short-range of the liquid reconstructed by accurate multiple-scattering XAS data-analysis.  
 → Pair and angular distributions obtained by Reverse Monte Carlo simulations (1372 atoms) using both XRD and XAS data, compared with results of accurate MD simulations

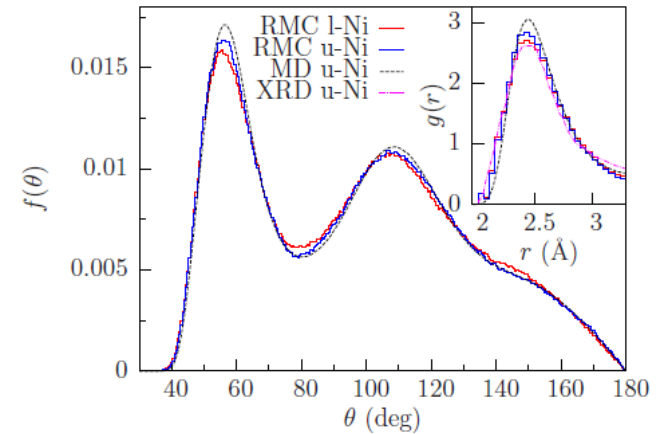


FIG. 3. Normalized bond angle distributions  $f(\theta)$  calculated from MD (dashed) and RMC configurations for u-Ni (blue on-line) and l-Ni (red on-line). Inset: first peak of the pair distribution function  $g(r)$  obtained by RMC-XAS for l-Ni (red color on-line) and u-Ni (blue color on-line), compared with MD results (dashed) and previous XRD data [19] (dot-dashed).

# Local geometry in close-packing liquids

## Spherical harmonics invariants

Geometrical characterization of clusters through a set of spherical harmonics invariants (Steinhardt *et al.*, PRB 28, 784 (1982)) calculated for each atom of the simulation at any equilibrium configuration.

$$Q_{lm} \equiv Y_{lm}(\theta(\vec{r}), \phi(\vec{r})) \quad \bar{Q}_{lm} = \frac{1}{N_b} \sum_{\text{bonds}} Q_{lm}(\vec{r}) \quad Q_l \equiv \left[ \frac{1}{2l+1} \sum_{m=-l}^l |\bar{Q}_{lm}|^2 \right]^{1/2} \quad W_l \equiv \sum_{m_1+m_2+m_3=0} \begin{bmatrix} l & l & l \\ m_1 & m_2 & m_3 \end{bmatrix} \times \bar{Q}_{l_1 m_1} \bar{Q}_{l_2 m_2} \bar{Q}_{l_3 m_3}$$

TABLE I. Reduced invariants  $\hat{W}_l$ , calculated numerically, for the simple shapes whose quadratic and third-order invariants are cataloged in Fig. 2.

	$\hat{W}_4$	$\hat{W}_6$	$\hat{W}_8$	$\hat{W}_{10}$
icos		-0.169754		-0.093967
fcc	-0.159316	-0.013161	+0.058454	-0.090128
hcp	+0.134097	-0.012442	+0.051259	-0.079854
bcc	+0.159317	+0.013161	-0.058455	-0.090130
sc	+0.159317	+0.013161	+0.058455	+0.090130

$$\hat{W}_l \equiv \frac{W_l}{\sum_{l=-m}^m [|\bar{Q}_{lm}|^2]^{3/2}}$$

● fcc  $\rightarrow \hat{W}_6 = -0.013161$

● icosahedron  $\rightarrow \hat{W}_6 = -0.169754$   
( $\hat{W}_l = 0$  if  $l < 6$ )

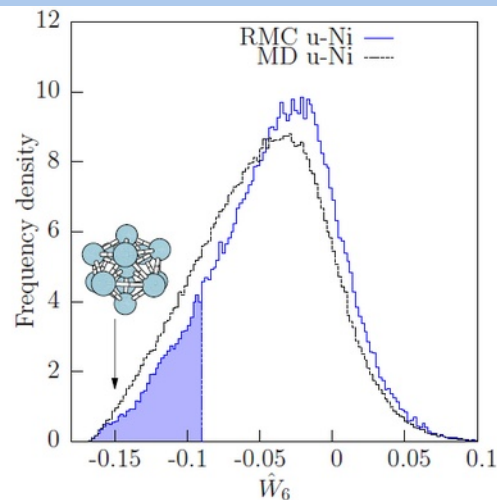
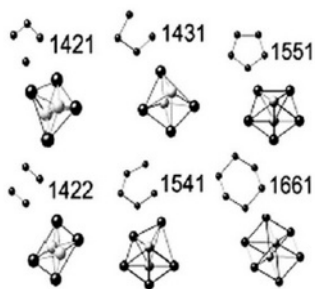


FIG. 5. (Color online) Normalized distribution of the spherical invariant  $\hat{W}_6$  calculated from MD and RMC configurations in u-Ni.

## Common neighbor analysis



Different type of pairs are associated with different type of local order  
 1421 and 1422 - fcc and hcp  
 1431 and 1541 - defective and distorted icosahedra  
 1551 - icosahedra  
 1661 - bcc

*RMC-XAS results validated also by MD simulations*

Trend of icosahedral ordering in different close-packing liquids probed by XAS: significantly reduced in liquid Cd (hcp with anomalous c/a ratio in the solid phase)

		I-Ni (1733 K)	I-Cu (1398 K)	I-Cd (613 K)
1421 + 1422	fcc/hcp	16%	15%	19%
1431 + 1541	def./dis. ico	40%	38%	34%
1551	ico	11%	10%	7%
1661	bcc	3%	3%	2%

Icosahedral ordering tends to increase in the undercooled phase

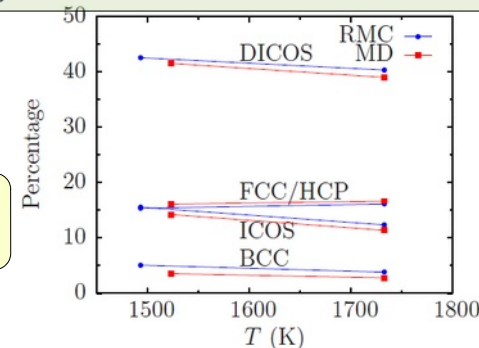


FIG. 4. (Color online) Percentage of nearest-neighbors pairs with given symmetry (CNA analysis of MD and RMC configurations). ICOS, icosahedral (555 pairs); DICOS, distorted icosahedral (544 and 433 pairs); BCC, bcc (666 pairs); and FCC/HCP, fcc and hcp (421 and 422 pairs).

# Polymorphism at high pressure: Sn

Polymorphic solid → polymorphic liquid?  
Undercooling at high pressure?  
Metastable solid states?  
Tin, an “easy” example..

Sn-II (diamond structure) ⇒ Sn-I ( $\beta$ -Sn tetragonal structure) ⇒ Sn-III (bct tetragonal)

Polymorphism in the solid phase:

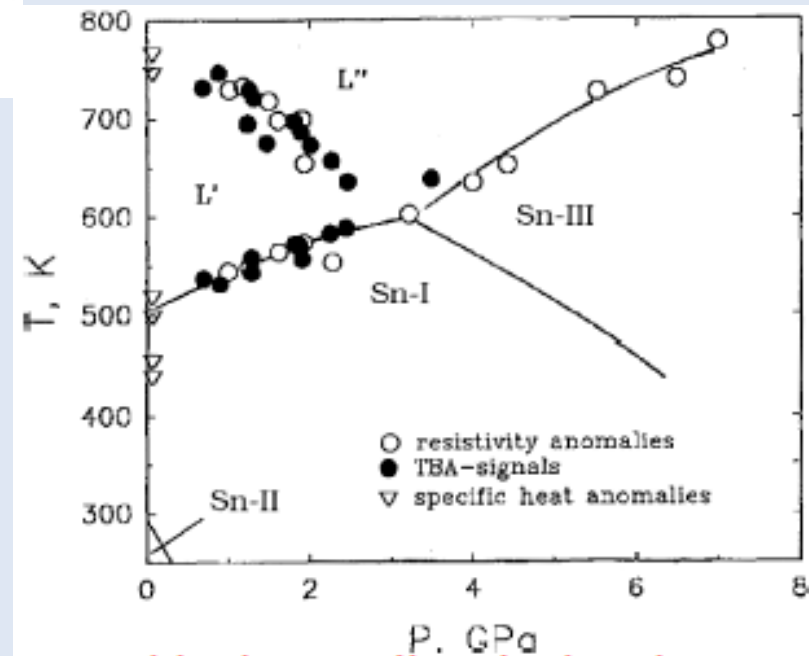
- phase Sn-II (or  $\alpha$ -Sn) (diamond structure)  $T < 291$  K - ambient pressure
- phase Sn-I (or  $\beta$ -Sn) (structure bct(4))
- phase Sn-III (or  $\gamma$ -Sn)  $P > 9.4$  GPa-RT (structure bct(2))

**Pressure-induced changes in the liquid:**  
specific heat, resistivity and TBA signal anomalies associated with possible L-L phase transitions (V. V. Brazhkin et al., High Press. Res. 1997 (267))

→ differences in the local structure?

XAS/diffraction experiment under HP-HT:

- range of P-T accessible with a large volume press
- access to the undercooled state ⇒ pressure dependence of supercooling (T-scan)
- determination of local structure and symmetries (XAS + RMC)

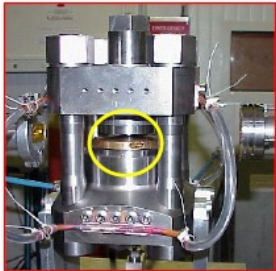




# Sn: undercooling and nucleation to metastable phases under pressure

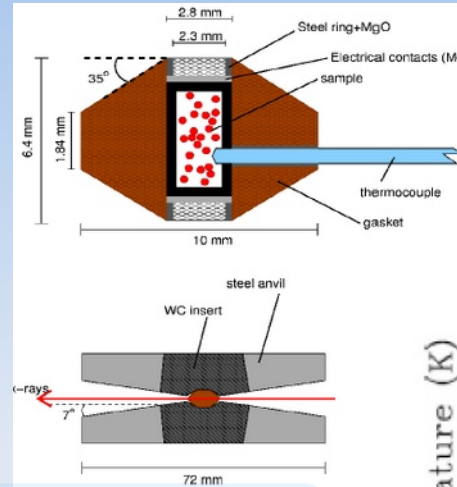
0-9 GPa ÷ 300-1800 K

"large volume"  $\approx 1 \text{ mm}^3$



Sn K-edge XAS experiment @ ESRF

Deep undercooling of Sn submicrometric grains (mixed with LiF and BN)

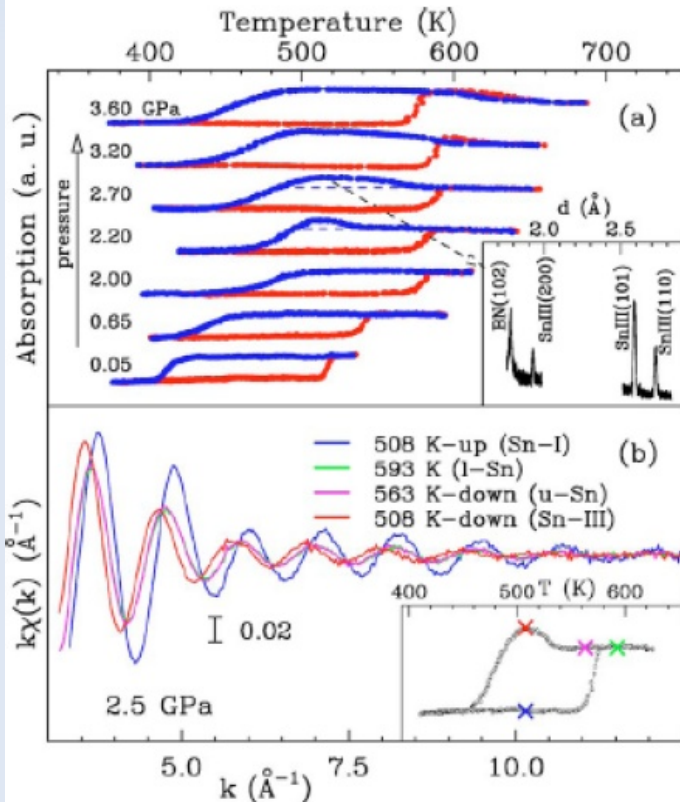


Sample micrometric powder

Mixture with suitable pressure markers (for example LiF)

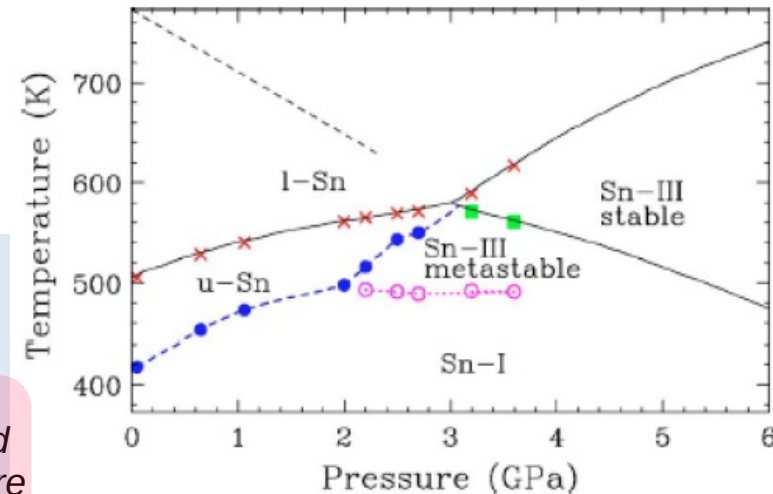
Graphite furnace

Present energy limit  $E > 8 \text{ keV}$



Temperature scans for increasing pressures

XAFS of liquid Sn, undercooled liquid and solid Sn-I and Sn-III are very different!



We observed an abrupt change in the undercooling limit of liquid Sn above 2 Gpa, where nucleation to the Sn-III metastable solid phase take place

# Liquid Sn: mixture of tetrahedral and close-packing configurations

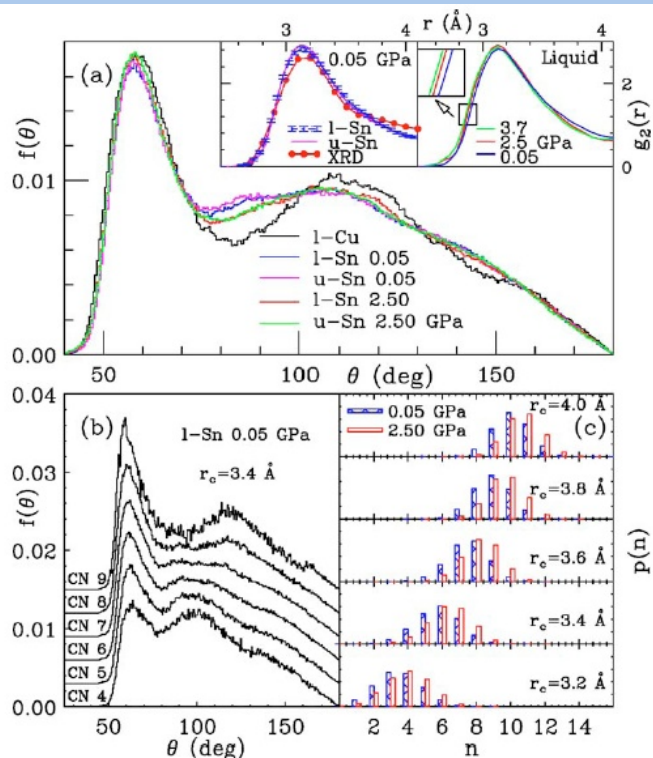
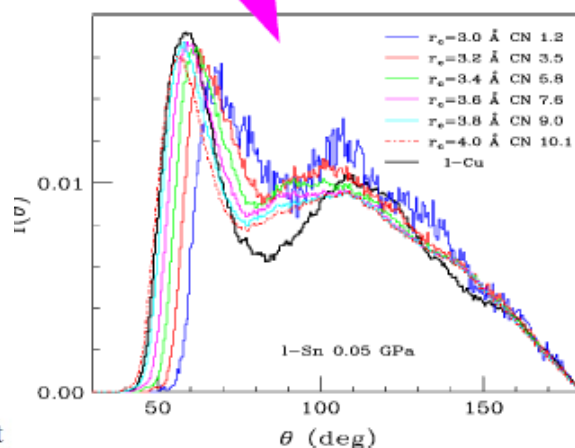


FIG. 3. (Color online) Panel (a): angular distributions of *l*-Sn and *u*-Sn at 0.05 and 2.5 GPa, where the nucleation of the Sn-III phase takes place. Inset (left): pair distribution functions of *l*-Sn and *u*-Sn compared with the  $g(r)$  measured by x-ray diffraction (Ref. 21). Error bars estimated from the RMC modeling are also shown. Inset (right):  $g(r)$  of *l*-Sn just above the melting temperature as a function of pressure. Panel (b): normalized angular distributions of liquid Sn at 0.05 GPa calculated around atoms having selected coordination numbers, within a sphere of radius 3.4 Å. Panel (c): probability distribution  $p(n)$  of the coordination numbers at 0.05 GPa (blue) and 2.5 GPa (empty red), for different cutoff values. The weight of high-coordinated configurations increases at high pressure.

- the angular distribution is visibly affected by the cut-off choice
- $f(\theta)$  is different from that of a “simple” liquid like Cu
- for lower cut-off increased weight of local configurations with  $\theta \approx 100^\circ$

•RMC-XAS



- Reverse Monte Carlo analysis of XAS data allowed us to reconstruct the short-range pair and three-body distributions.

- The liquid local structure is found to be composed of tetrahedral and close-packed configurations.
- The latter confs dominate at high pressure favoring crystallization to the Sn-III metastable solid phase.
- Details in A. D. C. et al., APL **89**, 221912 (2006). Ab-initio MD confirmed the gradual transition from an anisotropic to a nearly close-packed structure under pressure (Munejiri et al., JPCS **98** (2008) 042010)

# Conclusions

XAS techniques available at SR facilities useful for short-range structure refinement.

Atom-selective and use possible under various conditions (molecules, liquids, solids, interfaces, solutions...) also at low concentration

Advanced structural refinement is performed using multiple-scattering simulations (GNXAS)

Especially useful for disordered/ill-ordered matter (liquids, nanomaterials...) and dilute systems also under extreme conditions

# Acknowledgements

**Thanks for your attention!**

**Collaborators:**

Camerino XAS group (recent): M. Minicucci, A. Trapananti, S. J. Rezvani + students

National longstanding collaborations: A. Filipponi (L'Aquila), P. D'Angelo (Roma), C. R. Natoli (Frascati)

International collaborations: A. Polian (Soleil Saclay, IMPMC Paris), E. Mijiti (ESRF), K. Hatada (Toyama Univ.), F. Iesari (Aichi Synchrotron)

*Credits for several slides: all my collaborators*

# Additional slides

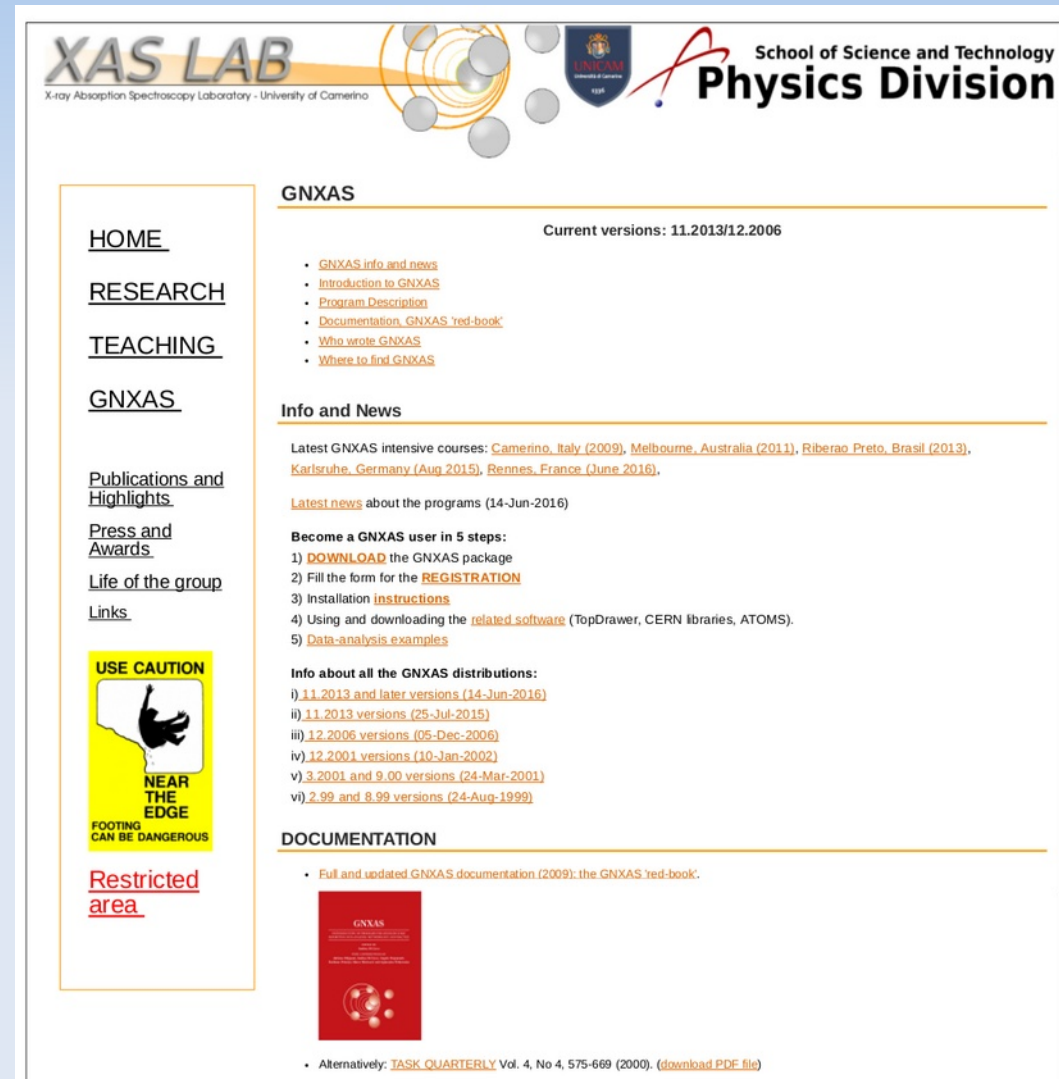
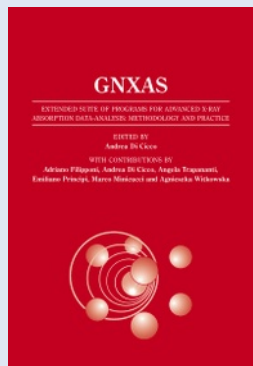
# Documentation

Guidelines for installation and usage are available at the website <http://gnxas.unicam.it>


Free downloading of executables)

Data analysis examples

Full documentation on GNXAS and related programs available (GnXAS red book 2009)



The screenshot shows the GNXAS website homepage. At the top, there is a header with the 'XAS LAB' logo (X-ray Absorption Spectroscopy Laboratory - University of Camerino), the 'UNICAM' logo, and the 'School of Science and Technology Physics Division' logo. The main content area is divided into several sections:

- HOME**
- RESEARCH**
- TEACHING**
- GNXAS**
  - Current versions: 11.2013/12.2006
  - Links: [GNXAS info and news](#), [Introduction to GNXAS](#), [Program Description](#), [Documentation, GNXAS 'red-book'](#), [Who wrote GNXAS](#), [Where to find GNXAS](#)
- Publications and Highlights**
- Press and Awards**
- Life of the group**
- Links**
- USE CAUTION** (Warning sign: NEAR THE EDGE, FOOTING CAN BE DANGEROUS)
- Restricted area**
- Info and News**
  - Latest GNXAS intensive courses: [Camerino, Italy \(2009\)](#), [Melbourne, Australia \(2011\)](#), [Ribeirao Preto, Brasil \(2013\)](#), [Karlsruhe, Germany \(Aug 2015\)](#), [Rennes, France \(June 2016\)](#).
  - [Latest news](#) about the programs (14-Jun-2016)
  - Become a GNXAS user in 5 steps:**
    - 1) **DOWNLOAD** the GNXAS package
    - 2) Fill the form for the **REGISTRATION**
    - 3) Installation **instructions**
    - 4) Using and downloading the **related software** (TopDrawer, CERN libraries, ATOMS).
    - 5) **Data-analysis examples**
  - Info about all the GNXAS distributions:**
    - i) **11.2013 and later versions (14-Jun-2016)**
    - ii) **11.2013 versions (25-Jul-2015)**
    - iii) **12.2006 versions (05-Dec-2006)**
    - iv) **12.2001 versions (10-Jan-2002)**
    - v) **3.2001 and 9.00 versions (24-Mar-2001)**
    - vi) **2.99 and 8.99 versions (24-Aug-1999)**
- DOCUMENTATION**
  - Full and updated GNXAS documentation (2009): the GNXAS 'red-book'.
  - Alternatively: **TASK QUARTERLY** Vol. 4, No 4, 575-669 (2000). ([download PDF file](#))